

Jamming II: Edwards' statistical mechanics of random packings of hard spheres

Ping Wang^a, Chaoming Song^a, Yuliang Jin^a, Hernán A. Makse^{a,*}

^a*Levich Institute and Physics Department, City College of New York, New York, NY 10031, US*

Abstract

The problem of finding the most efficient way to pack spheres has an illustrious history, dating back to the crystalline arrays conjectured by Kepler and the random geometries explored by Bernal in the 60's. This problem finds applications spanning from the mathematician's pencil, the processing of granular materials, the jamming and glass transitions, all the way to fruit packing in every grocery. There are presently numerous experiments showing that the loosest way to pack spheres gives a density of $\sim 55\%$ (named random loose packing, RLP) while filling all the loose voids results in a maximum density of $\sim 63 - 64\%$ (named random close packing, RCP). While those values seem robustly true, to this date there is no well-accepted physical explanation or theoretical prediction for them. Here we develop a common framework for understanding the random packings of monodisperse hard spheres whose limits can be interpreted as the experimentally observed RLP and RCP. The reason for these limits arises from a statistical picture of jammed states in which the RCP can be interpreted as the ground state of the ensemble of jammed matter with zero compactivity, while the RLP arises in the infinite compactivity limit. We combine an extended statistical mechanics approach 'a la Edwards' (where the role traditionally played by the energy and temperature in thermal systems is substituted by the volume and compactivity) with a constraint on mechanical stability imposed by the isostatic condition. We show how such approaches can bring results that can be compared to experiments and allow for an exploitation of the statistical mechanics framework. The key result is the use of a relation between the local Voronoi volumes of the constituent grains (denoted the volume function) and the number of neighbors in contact that permits to simply combine the two approaches to develop a theory of volume fluctuations in jammed

*Corresponding author

Email address: hmakse@lev.cuny.cuny.edu (Hernán A. Makse)

matter. Ultimately, our results lead to a phase diagram that provides a unifying view of the disordered hard sphere packing problem and further shedding light on a diverse spectrum of data, including the RLP state. Theoretical results are well reproduced by numerical simulations that confirm the essential role played by friction in determining both the RLP and RCP limits. The RLP values depend on friction, explaining why varied experimental results can be obtained.

1. Introduction

Filling containers with balls is one of the oldest mathematical puzzles known to scientists. The study of disordered sphere packings raises an interesting problem: How efficient and uniform will spheres pack if assembled randomly? This problem has an important application in the jamming phenomenon, which takes place in particulate systems where all particles are in close contact with one another. The study of jammed granular media offers unexpected challenges in physics since the equilibrium statistical mechanics fail for these out-of-equilibrium systems. The goal of the present study is to develop an ensemble theory of volume fluctuations to describe the statistical mechanics of jammed matter with the aim of shedding light to the long-standing problem of characterizing random sphere packings.

1.1. Sphere packing problem

The study of sphere packing problem started four centuries ago when Johannes Kepler conjectured that the most efficient arrangement of spheres is the FCC lattice (an important part of the 18th problem proposed by Hilbert in 1900). Even though this is a tool used for centuries in fruit markets around the globe, nearly 400 years passed before this conjecture was considered a mathematical proof, which has been developed only recently by Hales [1] in a series of articles covering 250 pages supplemented by 3Gb of computer code to determine the best ordered packing through linear programming. The difficulty arises since in 3d it is not enough to look at the packing of one cell, but it is necessary to consider several Voronoi cells at once. That is, the packing that minimize the volume locally (the dodecahedron) does not tile the system globally. Such a situation does not arise in 2d, where the hexagonal packing minimizes the volume locally and globally; the equivalent of Kepler conjecture in 2d, which is also known as Thue's theorem, was proved long ago [2, 3].

The analogous problem for disordered packings has also an illustrious but unfinished history. This problem was initiated by the pioneering work of Bernal in the 1960's [4] (although earlier attempts can be found). The traditional view states that [5] "packings of spherical particles have been shaken, settled in different fluids and kneaded inside rubber balloons and all with no better results than a maximum density of 63%". This is the so-called random close packing RCP limit [4, 5, 6, 7, 8]. On the other hand, other experiments have shown that densities as low as 55% can be obtained in random loose packings, RLP [6, 8, 9].

While the two limits seem reproducible in various experiments and computer simulations, a mathematically-rigorous definition is still unavailable. Indeed it was conjectured [10] that the RCP conception is mathematically ill-defined and should be replaced by the maximally random jammed (MRJ) conception in terms of an ensemble of order parameters.

To this date there is no well-accepted physical explanation of this phenomenon, no well-accepted theoretical prediction of such density values and heated debates are still found in the literature regarding the existence of rigorous definitions of the RCP and RLP, the uniqueness of the RCP state and the nature of their state of randomness.

1.2. *Understanding Jamming*

One of the most important physical applications of the sphere packing problem is to understand the intrinsic geometrical structures of jammed systems. A great deal of research has been devoted by physicists to the properties of packings of granular materials and other jammed systems such as compressed emulsions, dense colloids and glasses [12, 11], due to their “out-of-equilibrium” nature. Generally speaking, there are three interrelated approaches to understand the nature of the jammed state of matter and its ensuing jamming transition :

(a) Statistical mechanics of jammed matter: The jammed phase is described with the ensemble of volume and force fluctuations proposed by Edwards [13, 14, 16, 15, 21, 17, 18, 20, 19]. Ideas from the physics of glasses provide interesting cross-fertilization between the jamming transition and the glass transition [22, 23, 24, 25].

(b) Critical phenomena of deformable particle: jamming is seen as a critical point at which observables such as pressure, coordination number and elastic moduli behave as power-law near the critical volume fraction, ϕ_c , [26, 27, 29, 31, 32, 30, 28, 33, 34]. The jammed state is modelled as granular media composed of soft particles, typically Hertz-Mindlin [32, 35, 36] grains under external pressure and emulsions compressed under osmotic pressure [37], as they approach the jamming transition from the solid phase above the critical density: $\phi \rightarrow \phi_c^+$.

(c) Hard-sphere glasses: In parallel to studies in the field of jamming there exists a community attempting to understand the packing problem approaching jamming from the liquid phase [38, 39, 40], that is, $\phi \rightarrow \phi_c^-$. Here, amorphous jammed packings are seen as infinite pressure glassy states [38, 41]. Therefore, the properties of the jamming transition are intimately related to those of the glass transition [38].

A great deal of effort has been devoted to the study of jamming applying these approaches. A large body of experiments and simulations have fully characterized the jammed state in the critical phenomena framework of soft-particles. The hard-sphere field studies frictionless amorphous packings interacting with hard-core normal forces only. Their results are a particular case of the more general problem of jammed matter composed of frictional and frictionless hard spheres as treated in the present work.

Statistical mechanics studies of jammed matter were initiated in 1989 with the work of Sir Sam Edwards. It was first recognized that the main theoretical difficulty to develop a statistical formulation results from the lack of well-defined conservation laws on which an ensemble description of jammed matter could be based. Unlike equilibrium statistical mechanics where energy conservation holds, granular matter dissipates energy through frictional inter-particle forces. Therefore, it is doubtful that energy in granular matter could describe the microstates of the system and a new ensemble needs to be considered.

Stemming from the fact that it is possible to explore different jammed configuration at a given volume in systematic experiments [18, 42, 20, 19], Edwards proposed the volume ensemble (V-ensemble) as a replacement of the energy ensemble in equilibrium systems. A simple experiment is merely pouring grains in a fixed volume and applying perturbations, sound waves or gentle tapping, to explore the configurational changes. Concomitant with a given network geometry there is a distribution of contact forces or stresses in the particulate medium. This means that the V-ensemble must be supplemented by the force or stress ensemble (F-ensemble) determined by the contact forces [16, 43, 44] for a full characterization of jammed matter.

Following this theoretical framework, a large body of experiments, theory and simulations [13, 14, 16, 15, 21, 17, 18, 20, 19, 46, 47, 45, 37] have focused on the study of volume fluctuations in granular media. Statistical studies have been concerned with testing for the existence of thermodynamics quantities such as effective temperatures and compactivity as well as challenging the foundations based on the ergodic hypothesis or equal probability of the jammed states. It is recognized that thermodynamic analogies may illuminate methods for attempting to solve certain granular problems, but will inevitably fail at some point in their application. The mode of this failure is an interesting phenomenon, as the range of phenomena for which ergodicity of some kind or other will apply or not is an interesting question. This has been illustrated by the compaction experiments of the groups of Chicago, Texas, Rennes and Schlumberger [18, 42, 20, 19]. They have shown that reversible states exist along a branch of compaction curve where statistical mechanics is more likely to work. Conversely, experiments also showed a branch of irreversibility where the statistical framework is not expected to work. Poorly consolidated formations, such as a sandpile, are irreversible and a new “out-of-equilibrium” theory is required to describe them.

In this paper we will describe the reversible states which are amenable to the ergodic hypothesis while the unconsolidated irreversible states will be addressed in a future work. Unfortunately, there is no first principle derivation of the granular statistical mechanics analogous to the Liouville theorem for equilibrium systems [48]. Therefore, advancing the statistical mechanics of granular matter requires well-defined theoretical predictions that can be tested experimentally or numerically. While the possibility of a thermodynamic principle describing jammed matter is recognized as a sensible line of research, the problem with the statistical approach is that after almost 20 years there are no practical applications yet. We require predictions of practical importance such as equations of state relating the observables: pressure, volume, coordination

number, entropy, etc, that may lead to new phenomena to be discovered and tested experimentally that will allow for a concrete exploitation of the thermodynamic framework.

1.3. Objectives

Here, we explore this problem by developing a systematic study of the V-ensemble of jammed matter. Our systems of interest are primarily packings of granular materials, frictional colloids, infinitely rough grains and frictionless droplets mimicking concentrated emulsions. We attempt to answer the following questions using statistical mechanics methods:

- What is a jammed state?
- What are the proper state variables to describe the granular system at the ensemble level?
- What are the ensuing equations of state to relate the different observables? For instance, the simplest equilibrium thermal system, the ideal gas, is described by pressure, volume and temperature (p, V, T) through $pV = nRT$. Is it possible to identify the state variables for jammed matter which can describe the system in a specified region of the phase space?
- Which are the states with the maximum and minimum entropy (most and least disordered)?
- Can we define a "compactimeter" to measure compactivity?
- Can we provide a statistical interpretation of RLP and RCP, and use the ensemble formalism to predict their density values?

To answer these questions, we illuminate a diverse spectrum of data on sphere packings through a statistical theory of disordered jammed systems. Our results ultimately lead to a phase diagram providing a unifying view of the disordered sphere packing problem. An extensive program of computer simulations of frictional and frictionless granular media tests the predictions and assumptions of the theory, finding good general agreement. The phase diagram introduced here allows the understanding of how random packings fill space in 3d for any friction, and eventually can be extended as a mathematical model for packings in 2d and in higher dimensions, anisotropic particles and other systems. While physical application may be limited to 2d or 3d, higher dimensions find application in the science of information theory, where data transmission and encryption find use for packing optimization.

1.4. Outline

This paper is the second installment of a series of papers dealing with different aspects of jammed matter from a statistics mechanics point of view. In a companion paper, Jamming I [49], we describe the definition of the volume function based on the Voronoi volume of a particle and its relation to the coordination number.

In the present paper, Jamming II, we describe calculations leading to the phase diagram of jammed matter and numerical simulations to test the theoretical results; a short version of the present paper has been recently published in

[50]. Jamming III [51] describes the entropy calculation to characterize randomness in jammed matter and a discussion of the V-F ensemble. Jamming IV [52] studies the distribution of volumes from the mesoscopic ensemble point of view and a generalized z-ensemble to understand the distribution of coordination number. Jamming V [53] details the calculations for jamming in two dimensions at the mesoscopic level. The theory could be also extended to bidisperse [54] and high-dimensional systems [55].

The outline of the present paper is as follows: Section 2 explain the basis of the Edwards statistical mechanics. Section 3 summarizes the results of Jamming I regarding the calculation of the volume function. Section 4 describes the isostatic condition that defines the ensemble of jammed matter through the Θ_{jam} function, and explains the difference between the geometrical, z , and mechanical, Z , coordination number, which is important to define the canonical partition function. Section 5 defines the density of states in the partition function. Section 6 explains the main results of this paper in the equations of state (21) and (23), and the phase diagram of Fig. 4. Finally, Section 7 explains the numerical studies to test the theoretical predictions.

2. Statistical mechanics of jammed matter

Conventional statistical mechanics uses the ergodic hypothesis to derive the microcanonical and canonical ensembles, based on the quantities conserved, typically the energy E [48]. Thus the entropy in the microcanonical ensemble is $S(E) = k_B \log \int \delta(E - \mathcal{H}(p, q)) dpdq$, where $\mathcal{H}(p, q)$ is the Hamiltonian. This becomes the canonical ensemble with $\exp[-\mathcal{H}(\partial S/\partial E)]$.

The analogous development of a statistical mechanics of granular and other jammed materials presents many difficulties. Firstly, the macroscopic size of the constitutive particles forbids the equilibrium thermalization of the system. Secondly, the fact that energy is constantly dissipated via frictional interparticle forces further renders the problem outside the realm of equilibrium statistical mechanics due to the lack of energy conservation. In the absence of energy conservation laws, a new ensemble is needed in order to describe the system properties.

Following this theoretical perspective, Edwards proposed the statistical mechanics of jammed matter and interest in the problem of volume fluctuations has flourished [14]. The central concept is that of a volume function \mathcal{W} replacing the role of the Hamiltonian in describing the microstates of the system in the V-ensemble and the stress boundary

$$\Pi_{ij} = \int \sigma_{ij} dV$$

with the stress $\sigma_{ij} = 1/(2V) \sum_c f_i^c r_j^c$ describing the F-ensemble [16, 43, 44], where f_i^c, r_i^c are the force and position at contact c . For simplicity only the isotropic case is described. Thus, only the pressure $\sigma = \sigma_{ii}/3$ is necessary to describe force fluctuations.

If we partition the space associating each particle with its surrounding volume, \mathcal{W}_i (for instance with a Voronoi tessellation as it will be done below), then the total volume, \mathcal{W} , of a system of N particles is given by:

$$\mathcal{W} = \sum_{i=1}^N \mathcal{W}_i. \quad (1)$$

The ensemble average of the volume function \mathcal{W} provides the volume of the system, $V = \langle \mathcal{W} \rangle$, in an analogous way to the average of the Hamiltonian is the energy in the canonical ensemble of equilibrium statistical mechanics.

The full canonical partition function in the V-F ensemble is the starting point of the statistical analysis [16]:

$$\mathcal{Z}(X, A) = \int g(\mathcal{W}, \Pi) \exp \left[-\frac{\Pi}{A} - \frac{\mathcal{W}}{X} \right] \Theta_{\text{jam}} d\mathcal{W} d\Pi, \quad (2)$$

where $g(\mathcal{W}, \Pi)$ is the density of states for a given volume and boundary stress. Here Θ_{jam} formally imposes the jamming restriction and therefore defines the ensemble of jammed matter. This crucial function will be discussed at length below. As a minimum requirement it should ensure touching grains, and obedience to Newton's force laws.

Just as $\partial E / \partial S = T$ is the temperature in equilibrium systems, the temperature-like variables in granular systems are the compactivity [14]:

$$X = \frac{\partial V}{\partial S}, \quad (3)$$

and the angoricity [from the Greek “ἀγκος” (ankhos) = stress] [16]¹:

$$A = \frac{\partial \Pi}{\partial S}. \quad (4)$$

The compactivity measures the power to compactify while the angoricity measures the power to stress. These quantities have remained quite abstract so far, perhaps, this fact being the primary reason for the great deal of controversy surrounding the statistical mechanics of jammed matter. In the present paper we attempt to provide a meaning and interpretation for the compactivity (the angoricity will be treated in subsequent papers) by developing equations of states as well interpretations in terms of a “compactimeter” to measure the “temperature” of jammed matter. In Eq. (2), the analogue of the Boltzmann constant are set to unity for simplicity, implying that the compactivity is measured in units of volume and the angoricity in units of boundary stress (stress times volume).

¹Note that in [16], the angoricity is denoted Z . Here we use A for the isotropic angoricity since Z is used to denote the mechanical coordination number. In general the angoricity is a tensor, $A_{ij} = \frac{\partial \Pi_{ij}}{\partial S}$, here we simplify to the isotropic case.

In the limit of vanishing angoricity, $A \rightarrow 0$, the system is described by the V-ensemble alone. This is the hard sphere limit which will be the focus of the present work where the following partition function describes the statistics:

$$\mathcal{Z}_{\text{sph}}^{\text{hard}}(X) = \int g(\mathcal{W}) e^{-\mathcal{W}/X} \Theta_{\text{jam}} d\mathcal{W}, \quad (5)$$

where $g(\mathcal{W})$ is the density of states for a given volume \mathcal{W} .

3. Volume Function

While it is always possible to measure the total volume of the system, it is unclear how to partition the space to associate a volume to each grain. Thus, the first step to study the V-ensemble is to find the volume function \mathcal{W}_i associated to each particle that successfully tiles the system. This is analogous to the additive property of energy in equilibrium statistical mechanics. This derivation is explained in Jamming I [49] and is the main theoretical result that leads to the solution of the partition function for granular matter. We refer to this paper for details. Here we just state the main two results, Eqs. (6) and (7), and explain their significance for the solution of the statistical problem.

Initial attempts at modelling \mathcal{W} included, (a) a model volume function under mean-field approximation [14], (b) the work of Ball and Blumenfeld [56, 15] in 2d and in 3d [57], and (c) simpler versions in terms of the first coordination shell by Edwards [45]. These definitions are problematic: (a) is not given in terms of the contact network, (c) is not additive, (b) and (c) are proportional to the coordination number of the balls contrary to expectation (see below). In Jamming I [49] we have found an analytical form of the volume function in any dimensions and demonstrated that it is the Voronoi volume of the particle.

The definition of a Voronoi cell is a convex polygon whose interior consists of all points closer to a given particle than to any other (see Fig. 1). Its formula in terms of particle positions for monodisperse spherical packings in 3d is [49]:

$$\mathcal{W}_i^{\text{vor}} = \frac{1}{3} \left\langle \left(\frac{1}{2R} \min_j \frac{r_{ij}}{\cos \theta_{ij}} \right)^3 \right\rangle_s \equiv \langle \mathcal{W}_i^s \rangle_s, \quad (6)$$

where \vec{r}_{ij} is the vector from the position of particle i to that of particle j , the average is over all the directions \hat{s} forming an angle θ_{ij} with \vec{r}_{ij} as in Fig. 1, and R is the radius of the grain. \mathcal{W}_i^s defines the orientational Voronoi volume which is obtained without the integration over \hat{s} . This formula has a simple interpretation depicted in Fig. 1.

The Voronoi construction is additive and successfully tiles the total volume. Prior to Eq. (6), there was no analytical formula to calculate the Voronoi volume in terms of the contact network r_{ij} . Equation (6) provides such a formula which allows theoretical analysis in the V-ensemble. However this microscopic version is difficult to incorporate into the partition function since it would necessitate a field theory. The next step is to develop a theory of volume fluctuations to coarse

grain \mathcal{W}_i^{vor} over a mesoscopic length scale and calculate an average volume function. The coarsening reduces the degrees of freedom to one variable, the coordination number of each grain, and defines a mesoscopic volume function which is more amenable to statistical calculations than Eq. (6). We find a (reduced) free volume function [49]:

$$w(z) \equiv \frac{\langle \mathcal{W}_i^s \rangle_i - V_g}{V_g} \approx \frac{2\sqrt{3}}{z}, \quad (7)$$

approximately valid for monodisperse hard spheres with volume V_g , where z is the geometrical coordination number (which is different from the mechanical coordination number, Z , see below). The average is over all the balls.

The inverse relation with z in Eq. (7) is in general agreement with experiments [46]. Many experiments have focused on the analysis of the system volume and single particle volume fluctuations in granular media [19, 46, 47, 18]. Of particular importance to the present theory are the recent advances in X-ray tomography [46] and confocal microscopy [37, 58] which have revealed the detailed internal structure of jammed matter allowing for the study of the free volume per particle. By partitioning the space with Voronoi diagrams, these studies show that \mathcal{W}_i^{vor} is distributed with wide tails [46, 47, 45, 37]. More importantly, the X-ray tomography experiments with 300,000 monodisperse hard spheres performed by the Aste group [46] find that the Voronoi volumes are inversely proportional, on average, to the coordination number of the particle, z , in reasonable agreement with the prediction of the volume function Eq. (7). Such data is displayed in Fig. 6 in [46] where the local volume fraction defined as $\phi_i^{-1} - 1 = \mathcal{W}_i^{vor}/V_g$ is plotted against the coordination number. From Eq. (7) we find:

$$\phi_i = \frac{1}{w + 1} = \frac{z}{z + 2\sqrt{3}}, \quad (8)$$

which agrees relatively well with the shape of the curves displayed in Fig. 6 of [46] for different packing preparations. It should be noted that for a more precise comparison a coarse grained volume fraction and geometrical coordination number should be considered in Eq. (8). A detailed discussion is provided in Section 7.6.

The free volume function decreases with z as expected since the more contacts per grain, the more jammed the particle is and the smaller the free volume associated with the grain. The coordination number z in Eq. (7) can be considered as a coarse-grained average associated with “quasiparticles” with mesoscopic free volume w . By analogy to the theory of quantum energy spectra, we regard each state described by Eq. (7) as an assembly of “elementary excitations” which behave as independent quasiparticles. As a grain is jammed in the packing, it interacts with other grains. The role of this interaction between grains is assumed in the calculation of the volume function (7) and it is implicit in the coarse-graining procedure explained above. The quasiparticles can be considered as particles in a self-consistent field of surrounding jammed matter.

In the presence of this field, the volume of the quasiparticles depends on the surrounding particles as expressed in Eq. (6). The assembly of quasiparticles can be regarded as a set of non-interacting particles (when the number of elementary excitations is sufficiently low) and a single particle approximation can be used to solve the partition function as we will formulate in Section 6.

While Eq. (6) is difficult to treat analytically, the advantage of the mesoscopic Eq. (7) is that the partition function can be solved analytically since w depends on z only, instead of r_{ij} . The key result is the relation between the Voronoi volume and the coordination number which allow us to incorporate the volume function into a statistical mechanics approach of jammed hard spheres, by using the constraint of mechanical stability as we show below.

4. Definition of jamming: isostatic conjecture

The definition of the constraint function Θ_{jam} is intimately related to the proper definition of a jammed state and should contain the minimum requirement of mechanical equilibrium.

Distinguishing between metastable and mechanically stable packings that define the jammed state through the Θ_{jam} function remains a problem under debate, related to the more fundamental question of whether or not a jammed packing is well-defined [10]. In practice, it is widely believed that the isostatic condition is necessary for a jammed disordered packing following the Alexander conjecture [59, 60, 61] which was tested in several works [27, 29, 30, 33]

It is well known that mechanical equilibrium imposes an average coordination number larger or equal than a minimum coordination where the number of force variables equals the number of force and torque balance equations [59, 61, 60]. The so-called isostatic condition.

In the case of frictionless spherical particles the isostatic condition is $Z = 2d = 6$ (in 3d), while the coordination in the case of infinitely rough particles (with interparticle friction coefficient $\mu \rightarrow \infty$) is $Z = d + 1 = 4$, where d is the dimension of the system. Numerical simulations and theoretical work suggest that at the jamming transition the system becomes exactly isostatic [29, 31, 27, 34, 61, 33, 60]. But no rigorous proof of this statement exists. In the following, we will use this isostatic conjecture to define the ensemble of jammed matter.

While isostaticity holds for perfectly smooth and infinitely rough grains, the main problem is to extend it to finite frictional systems. For finite friction, the Coulomb condition takes the form of an inequality between the normal interparticle contact force F_n and the tangential one F_t : $F_t \leq \mu F_n$ and therefore no trivial solution to the minimum number of contacts can be obtained.

The problem can be understood as an optimization of an outcome based on a set of constraints, i.e., minimizing a Hamiltonian of a system over a convex polyhedron specified by linear and non-negativity constraints. The isostatic condition can be augmented to indicate the number of extra equations for contacts satisfying the Coulomb condition, which is analogous to the number of

Table 1: Number of constraints and variables determining the isostatic condition for different systems of spherical particles.

Friction	N_n	N_t	E_f	E_t
$\mu = 0$	$\frac{1}{2}NZ$	0	dN	0
μ finite	$\frac{1}{2}NZ$	$\frac{1}{2}(d-1)NZf_2(\mu)$	dN	$\frac{1}{2}d(d-1)Nf_1(\mu)$
$\mu = \infty$	$\frac{1}{2}NZ$	$\frac{1}{2}(d-1)NZ$	dN	$\frac{1}{2}d(d-1)N$

redundant constraints in Maxwell constraint counting of rigidity percolation. This suggests that, for a finite value of μ , the original nonlinear problem can be mapped to a linear equation problem if we know how many extra equations should be added. This problem is treated with more details in a future paper.

In the following, we present a rough approximation suggesting that the coordination number could be related to friction. We consider the following argument. Consider a set of spherical particles interacting via normal and tangential contact forces. These can be the standard Hertz and Mindlin/Coulomb forces of contact mechanics [35, 36, 32], respectively, see Section 7.1. We set N : number of particles, N_n : number of unknown normal forces, N_t : number of unknown tangential forces, E_f : number of force balance equations, E_t : number of torque balance equations, $Z = 2M/N$: average coordination number of the packing, where M is the total number of contacts, $f_1(\mu)$: undetermined function of the friction coefficient μ such that $1 - f_1(\mu)$ is the fraction of spheres that can rotate freely ($f_1(0) = 0$ and $f_1(\infty) = 1$), and $f_2(\mu)$: undetermined function of μ indicating the ratio of contacts satisfying $F_t < \mu F_n$, which satisfies $f_2(0) = 0$ and $f_2(\infty) = 1$.

A packing is isostatic when

$$N_n + N_t = E_f + E_t. \quad (9)$$

The average coordination number at the isostatic point is then (see Table 1):

$$Z(\mu) = 2d \frac{1 + 1/2(d-1)f_1(\mu)}{1 + (d-1)f_2(\mu)}, \quad (10)$$

reducing to the known $Z = 2d$ for frictionless particles and $Z = d + 1$ for infinitely rough particles.

In what follows, we use the numerical fact that interpolating between the two isostatic limits, there exist packings of finite μ with the coordination number smoothly varying between $Z(\mu = 0) = 6$ and $Z(\mu \rightarrow \infty) \rightarrow 4$ [30]. Numerical simulations with packings described in Section 7 corroborate this result and further show that the Z vs μ dependence is independent of the preparation protocol as obtained in our simulations (see Fig. 2). This result then generalizes the isostatic conditions from $\mu = 0$ and $\mu = \infty$ to finite μ .

It should be noted that we cannot rule out that other preparation protocols could give rise to other dependence of Z on μ . However, we will see that the

obtained phase diagram is given in terms of Z ; the main prediction of the theory would still be valid irrespective of the particular dependence $Z(\mu)$. That is, the theory does not assume anything about the relation between the interparticle friction and Z .

It is worth noting that other attempts to define the jammed state have been developed. A rigorous attempt is that of Torquato *et al.* who propose three categories of jamming [62]: locally jammed, collectively jammed and strictly jammed based on geometrical constraints. However, the definition of [62] is based purely on geometrical considerations and therefore only valid for frictionless particles. Thus it is not suitable for granular materials with inter-particle frictional tangential forces; their configurational space is influenced by the mechanics of normal and shear forces. Other approaches to define a jammed state based on the potential energy landscape [29] fail for granular materials too since such a potential does not exist for frictional grains due to their inherent path-dependency. Thus, the definition of jammed state for granular materials must consider interparticle normal and tangential contact forces beyond geometry. In the companion paper [51] we elaborate on this problem.

4.1. Geometrical and mechanical coordination number

We have acknowledged a difference between the geometrical coordination number z in Eq. (7) and the mechanical coordination number Z which counts only the contacts with non-zero forces. Below we discuss the bounds of z .

Since some geometrical contacts may carry no force, then we have:

$$Z \leq z. \quad (11)$$

To show this, imagine a packing of infinitely rough ($\mu \rightarrow \infty$) spheres with volume fraction close to 0.64. There must be $z = 6$ nearest neighbors around each particle on the average. However, the mechanical balance law requires only $Z = 4$ contacts per particle on average, implying that 2 contacts have zero force and do not contribute to the contact force network.

Such a situation is possible as shown in Fig. 3: starting with the contact network of an isostatic packing of frictionless spheres having $Z = 6$ and all contacts carrying forces (then $z = 6$ also as shown in Fig. 3a), we simply allow the existence of tangential forces between the particles and switch the friction coefficient to infinity. Subsequently, we solve the force and torque balance equations again for this modified packing of infinitely rough spheres but same geometrical network, as shown in Fig. 3b [Notice that the shear force is composed of an elastic Mindlin component plus the Coulomb condition determined by μ , see Section 7.1 for details. Thus when $\mu \rightarrow \infty$, the elastic Mindlin component still remains].

The resulting packing is mechanically stable and is obtained by setting to zero the forces of two contacts per ball, on average, to satisfy the new force and torque balance condition for the additional tangential force at the contact. Such a solution is guaranteed to exist due to the isostatic condition: at $Z = 4$ the number of equations equals the number of force variables. Despite mechanical

equilibrium, giving $Z = 4$, there are still $z = 6$ geometrical contacts contributing to the volume function.

Therefore, we identify two types of coordination number: the geometrical coordination number, z , contributing to the volume function and the mechanical coordination number, Z , measuring the contacts that carry forces only. This distinction is crucial to understand the sum over the states and the bounds in the partition function as explained below.

These ideas are corroborated by numerical simulations in Section 7.6, below. The packings along the vertical RCP line found in the simulations (see Fig. 11) have approximately the same geometrical coordination number, $z \approx 6$. However, they differ in mechanical coordination number, going from the frictionless point $Z = 6$ to $Z \approx 4$ as the friction coefficient is increased to infinity.

We have established a lower bound of the geometrical coordination in Eq. (11). The upper bound arises from considering the constraints in the positions of the rigid hard spheres. For hard spheres, the Nd positions of the particles are constrained by the $Nz/2$ geometrical constraints, $|\vec{r}_{ij}| = 2R$, of rigidity. Thus, the number of contacts satisfies $Nz/2 \leq Nd$, and z is bounded by:

$$z \leq 2d. \quad (12)$$

Notice that this upper bound applies to the geometrical coordination, z and not to the mechanical one, Z , and it is valid for any system irrespective of the friction coefficient, from $\mu = 0 \rightarrow \infty$.

Furthermore, in relation with the discussion of frictionless isostaticity, it is believed that above $2d$, the system is partially crystallized. To increase the coordination number above 6, it is necessary to create partial crystallization in the packing, up to the point of full order of the FCC lattice with coordination number 12. Thus, by defining the upper bound at the frictionless isostatic limit we also exclude from the ensemble the partially crystalline packings. This is an important point, akin to mathematical tricks employed in replica approaches to glasses [38].

In conclusion, the mechanical coordination number, Z , ranges from 4 to 6 as a function of μ , and provides a lower bound to the geometrical coordination number, while the upper bound is $2d$. A granular system is specified by the interparticle friction which determines the average mechanical coordination at which the system is equilibrated, $Z(\mu)$. The possible microstates in the ensemble available for this system follow a Boltzmann distribution Eq. (5) for states satisfying the following bounds:

$$Z(\mu) \leq z \leq 2d = 6. \quad (13)$$

5. Density of states

According to the statistical mechanics of jammed matter, the volume partition function \mathcal{Z} is defined by Eq. (5). In the quasiparticle approximation we can write:

$$\mathcal{Z}_{\text{sph}}^{\text{hard}}(X) = \int \dots \int g\left(\sum w(z_i)\right) e^{-\sum w(z_i)/X} \times \\ \times \Theta_{\text{jam}} \prod_i^N dw(z_i). \quad (14)$$

Considering N non-interacting quasiparticles with free volume $w(z)$, the partition function can be written as:

$$\mathcal{Z}_{\text{sph}}^{\text{hard}} = \left(\int g(w) e^{-w/X} \Theta_{\text{jam}} dw \right)^N. \quad (15)$$

Here, $g(w)$ is the density of states for a given quasiparticle free volume.

Since the mesoscopic w is directly related to z through Eq. (7), we change variables to the geometrical coordination number in the partition function. The density of states for a single quasiparticle, $g(w)$, is:

$$g(w) = \int_z^6 P(w|z)g(z)dz, \quad (16)$$

where $P(w|z)$ is the conditional probability of a free volume w for a given z , and $g(z)$ is the density of states for a given z . Here, we have used the bounds in Eq. (13).

The next step in the derivation is the calculation of $g(z)$ which is developed in three steps:

First, we consider that the packing of hard spheres is in a jammed configuration where there can be no collective motion of any contacting subset of particles leading to unjamming when including the normal and tangential forces between the particles. This definition is an extended version of the collectively jammed category proposed by Torquato *et al.* [62] that goes beyond the merely locally jammed configuration of packings, unstable to the motion of a single particle. While the degrees of freedom are continuous, the fact that the packing is collectively jammed implies that the jammed configurations in the volume space are not continuous. Otherwise there would be a continuous transformation in the position space that would unjam the system contradicting the fact that the packing is collectively jammed.

Thus, we consider that the configuration space of jammed matter is discrete since we cannot change one configuration to another in a continuous way. Similar consideration of discreteness has been studied in [62]. Notice that the volume landscape could be continuous since we could change the volume as well, or, in the case of soft particle, we can deform them. Additionally, in the case of frictionless packings of soft particle, the energy of deformation is well-defined, and we can define the collectively jammed configuration as a minimum in the energy with definitive positive Hessian (or a zero order saddle) like in [29]. In this case, there could be no continuous transformation of the particle coordinates

that brings one jammed state to the next, unless we deform the particles. Thus, the space is discrete in this case as well.

Second, we call the dimension per particle of the configuration space as \mathcal{D} and consider that the distance between two jammed configurations is not broadly distributed (meaning that the average distance is well-defined). We call the typical (average) distance between configurations in the volume space as h_z , and therefore the number of configurations per particle is proportional to $1/(h_z)^{\mathcal{D}}$. The constant h_z plays the role of the Planck's constant, h , in quantum mechanics.

Third, we add z constraints per particle due to the fact that the particle is jammed by z contacts. Thus, there are Nz position constrains ($|\vec{r}_{ij}| = 2R$) for a jammed state of hard spheres as compared to the unjammed "gas" state. Therefore, the number of degrees of freedom is reduced to $\mathcal{D} - z$, and the number of configurations is then $1/(h_z)^{\mathcal{D} - z}$. Since the term $1/(h_z)^{\mathcal{D}}$ is a constant, it will not influence the average of the observables in the partition function (although it changes the value of the entropy, see Jamming III [51]). Therefore, the density of states $g(z)$ is assumed to have an exponential form:

$$g(z) = (h_z)^z = e^{-z/z_c}, \quad (17)$$

with $z_c^{-1} \equiv \ln(1/h_z)$. Physically, we expect $h_z \ll 1$, then $g(z)$ is an exponentially rapid decreasing function with z . The exact value of h_z can be determined from a fitting of the theoretical values to the simulation data. The most populated state is the highest volume at $z = 4$ while the least populated state is the ground state at $z = 6$. A constant could be added in (17) but it has no consequence for the average of the observables in the partition function. However, it affect the value of the entropy. For the calculation of the entropy we consider that there is a single mesoscopic ground state and use $g(z) = e^{-(z-2d)/z_c}$ [51].

We see that the negative of the geometrical coordination number, $-z$, plays the role of a number of degrees of freedom for a packing, due to the extra position constrains of the contacting particles. The coordination z can be then considered as the number of degrees of "frozen" per particle. Another way to understand Eq. (17) is the following. In the case of a continuous phase space of configurations we would obtain $\frac{g(z+1)}{g(z)} = 0$. However, since the space of volume configurations is discrete as discussed above, the ratio $\frac{g(z+1)}{g(z)} \sim h_z$. This implies again Eq. (17).

The conditional probability $P(w|z)$ depends on the w function, $w = \frac{2\sqrt{3}}{z}$. The average is taken over a certain mesoscopic length scale since the volume of a particle depends on the positions of the particles surrounding it. Practically, such length scale is approximately of several particle diameters. w is a coarse-grained volume and independent of the microscopic partition of the particles, implying:

$$P(w|z) = \delta(w - 2\sqrt{3}/z). \quad (18)$$

The meaning of Eq. (18) is that we neglect the fluctuations in the coordination number due to the coarse graining procedure. A more general ensemble can be

considered where the fluctuations in the geometrical coordination number are taken into account. We have extended our calculations to consider fluctuations in z and find a similar phase diagram as predicted by the present partition function. This generalized z -ensemble will be treated in a future paper, where the boundaries of the phase diagram are regarded as a second-order phase transition. The generalized z -ensemble allows for the calculation of the probability distribution of the coordination number, beyond the assumption of the delta function distribution in Eq. (18). The resulting prediction of $P(z)$ is in general agreement with simulations (see [52]).

Substituting Eq. (18) and Eq. (17) into Eq. (15), we find the isostatic partition function which is used in the remaining of this study:

$$\mathcal{Z}_{\text{iso}}(X, Z) = \int_Z^6 (h_z)^z \exp\left(-\frac{2\sqrt{3}}{zX}\right) dz. \quad (19)$$

6. Phase diagram

Next, we obtain the equations of state to define the phase diagram of jammed matter by solving the partition function. From Eq. (19), we calculate the ensemble average volume fraction $\phi = (w + 1)^{-1} = z/(z + 2\sqrt{3})$ as:

$$\phi(X, Z) = \frac{1}{\mathcal{Z}_{\text{iso}}(X, Z)} \int_Z^6 \frac{z}{z + 2\sqrt{3}} \exp\left(-\frac{2\sqrt{3}}{zX} + z \ln h_z\right) dz. \quad (20)$$

We start by investigating the limiting cases of zero and infinite compactivity.

(a) In the limit of vanishing compactivity ($X \rightarrow 0$), only the minimum volume or ground state at $z = 6$ contributes to the partition function. Then we obtain the ground state of jammed matter with a density:

$$\phi_{\text{RCP}} = \phi(X = 0, Z) = \frac{6}{6 + 2\sqrt{3}} \approx 0.634, \quad Z(\mu) \in [4, 6]. \quad (21)$$

The meaning of the subscript RCP in (21) will become clear below.

(b) In the limit of infinite compactivity ($X \rightarrow \infty$), the Boltzmann factor $\exp[-2\sqrt{3}/(zX)] \rightarrow 1$, and the average in (20) is taken over all the states with equal probability. We obtain:

$$\begin{aligned} \phi_{\text{RLP}}(Z) &= \phi(X \rightarrow \infty, Z) = \\ &= \frac{1}{\mathcal{Z}_{\text{iso}}(\infty, Z)} \int_Z^6 \frac{z}{z + 2\sqrt{3}} \exp(z \ln h_z) dz. \end{aligned} \quad (22)$$

The constant h_z determines the minimum volume in the phase space. We expect $h_z \ll 1$, such that the exponential in Eq. (22) decays rapidly. Then

the leading contribution to Eq. (22) is from the highest volume at $z = Z$ and therefore:

$$\phi_{\text{RLP}}(Z) \approx \frac{Z}{Z + 2\sqrt{3}}, \quad Z(\mu) \in [4, 6]. \quad (23)$$

This dependence of the volume fraction on Z suggests using the (ϕ, Z) plane to define the phase diagram of jammed matter as plotted in Fig. 4. The equations of state (21) and (23) are plotted in the (ϕ, Z) plane in Fig. 4 providing two limits of the phase diagram. Since the mechanical coordination number is limited by $4 \leq Z \leq 6$ we have two more horizontal limits: The phase space is delimited from below by the minimum coordination $Z = 4$ for infinitely rough grains, denoted the granular-line or G-line in Fig. 4.

All mechanically stable disordered jammed packings lie within the confining limits of the phase diagram (indicated by the yellow zone in Fig. 4), while the grey shaded area in Fig. 4 indicates the forbidden zone. For example, a packing of frictional hard spheres with $Z = 5$ (corresponding to a granular material with interparticle friction $\mu \approx 0.2$ according to Fig. 2) cannot be equilibrated at volume fractions below $\phi < \phi_{\text{RLP}}(Z = 5) = 5/(5 + 2\sqrt{3}) = 0.591$ or above $\phi > \phi_{\text{RCP}} = 0.634$. It is worth noting that particular packings can exist in the forbidden zone; our contention is that they are zero measure and therefore have zero probability of occurrence at the ensemble level.

These results provide a statistical interpretation of the RLP and RCP limits:

(i) **The RCP limit.**— Stemming from the statistical mechanics approach, the RCP limit arises as the result of the relation (21), which gives the maximum volume fraction of disordered packings under the mesoscopic framework. To the right of the RCP-line, packings exist only with some degree of order (for instance with crystalline regions). The prediction,

$$\phi_{\text{RCP}} = \frac{6}{6 + 2\sqrt{3}} \approx 0.634, \quad (24)$$

is valid for all friction coefficients and approximates the experimental and numerical estimations [5, 6, 7, 8] which find a close packing limit independent of friction in a narrow range around 0.64.

Beyond the fact that 63-64% is commonly quoted as RCP for monodisperse hard spheres, we present a physical interpretation of that value as the ground state of frictional hard spheres characterized by a given interparticle friction coefficient. In this representation, as μ varies from 0 to ∞ and Z decreases from 6 to 4, the state of RCP changes accordingly while its volume fraction remains the same, given by Eq. (24). The present approach has led to an unexpected number of states that all lie in the RCP line from $Z = 6$ to $Z = 4$ as depicted in Fig. 4, suggesting that RCP is not a unique point in the phase diagram.

An important prediction is that for frictionless systems there is only one possible state at $Z = 6$. It is important to note that there is one state only at the mesoscopic level used in the theory. However, for a single mesoscopic state, we expect many microstates, which are averaged out in the mesoscopic theory

of the volume function. Thus, there could be more jammed states surrounding the frictionless point in the phase diagram. However, we expect that these states are clustered in a narrow region around the frictionless point. To access these microstates it would require different preparation protocols, analogous to the dependence of the glass transition temperature on cooling rates in glasses [40, 38].

It is interesting to note that replica approaches to the jammed states [38] predict many jammed isostatic states with different volume fractions for frictionless hard spheres. The first question is whether these states in the force/energy ensemble are the same as the volume ensemble states that we treat in our approach. It should be noted that jamming in [40, 38] is obtained when the particles are rattling infinitely fast in their cages, in the limit of infinite number of collisions per unit time. That is when the dynamic pressure related to the momentum of the particles diverges. Second, from our point of view, an investigation of the fluctuations of the microstates as well as more general ensembles allowing for fluctuations in the coordination number could be considered. These studies, may reveal whether the frictionless point is unique or not. This point is investigated further in Section 7.5.

(ii) **The RLP limit.**— Equation of state (23) provides the lowest volume fraction for a given Z and represents a statistical interpretation of the RLP limit depicted by the RLP-line in Fig. 4. We predict that to the left of this line, packings are not mechanically stable or they are experimentally irreversible as discussed in [18, 19, 20].

A review of the literature indicates that there is no general consensus on the value of RLP as different estimations have been reported ranging from 0.55 to 0.60 [6, 9, 8], proposing that there is no clear definition of RLP limit. The phase diagram proposes a solution to this problem. Following the infinite compactivity RLP-line, the volume fraction of the RLP decreases with increasing friction from the frictionless point $(\phi, Z) = (0.634, 6)$, towards the limit of infinitely rough hard spheres, $Z \rightarrow 4$. Indeed, experiments [6] indicate that lower volume fractions are achieved for larger coefficient of friction. We predict the lowest volume fraction in the limit: $\mu \rightarrow \infty$, $X \rightarrow \infty$ and $Z \rightarrow 4$ (and $h_z \rightarrow 0$) at

$$\phi_{\text{RLP}}^{\text{min}} = \frac{4}{4 + 2\sqrt{3}} \approx 0.536. \quad (25)$$

Even though this is a theoretical limit, our results indicate that for $\mu > 1$ this limit can be approximately achieved.

The finding of a random loose packing bound is an interesting prediction of the present theory. The RLP limit has not been well investigated experimentally, and so far it was not certain whether this limit can or cannot be reached in real systems. The lowest stable volume fraction ever reported, 0.550 ± 0.006 , obtained by Onoda and Liniger [9] as the limit of vanishing gravity for spherical glass beads, is not far from the present prediction.

The intersections of the RCP, RLP and the G-line identify three interesting points in the $(\phi, Z(\mu))$ plane:

(a) The frictionless point $\mu = 0$, denoted J-point in [29], at

$$J \equiv (\phi_{\text{RCP}}, Z(0)) = (0.634, 6),$$

corresponds to a system of compressed emulsions in the limit of small osmotic pressure as measured by J. Brujić [63].

(b) The lowest coordination number $Z = 4$ plotted as the G-line defines two associated points from the lowest volume fraction of loose packings at infinite compactivity, L-point,

$$L \equiv (\phi_{\text{RLP}}^{\text{min}}, Z(\infty)) = (0.536, 4),$$

to the zero compactivity state of close packing, C-point,

$$C \equiv (\phi_{\text{RCP}}, Z(\infty)) = (0.634, 4).$$

The full JCL triangle defines the isostatic plane where the frictional hard sphere packings reside.

(iii) **Intermediate isocompactivity states.**— For finite X , Eq. (20) can be solved numerically. For each X , the function $\phi(X, Z)$ can be obtained and is plotted as each isocompactivity color line in Fig. 4. Between the two limits Eqs. (21) and (23), there are packings inside the yellow zone in Fig. 4 with finite compactivity, $0 < X < \infty$. Since X controls the probability of each state, like in condensed matter through a Boltzmann-like factor in Eq. (5), it characterizes the number of possible ways to rearrange a packing having a given volume and entropy, S . Thus, the limit of the most compact and least compact stable arrangements correspond to $X \rightarrow 0$ and $X \rightarrow \infty$, respectively. Between these limits, the compactivity determines the volume fraction from RCP to RLP.

Dependence on h_z and negative compactivity.—

Of interest is the dependence of our prediction on the “Planck constant” of jammed matter, h_z , that determines the minimum volume in the phase space. The equation of state (23) and the prediction of the minimum RLP, Eq. (25) have been obtained by considering $h_z \rightarrow 0$ but still nonzero. Thus, when $X \rightarrow \infty$, the only state contributing to the volume partition function is the most populated at $z = Z(\mu)$.

The approximation $h_z \ll 1$ is a sensible one, since the discretization of the space is supposed to be very small. However, this constant remains a fitting parameter of the theory. Indeed in the simulations we will use a value of $h_z = e^{-100}$ in order to fit the theoretical values with the numerical ones for finite compactivity. This extremely small constant shifts the value of the minimum RLP a little bit to the right of the phase diagram from the prediction of Eq. (25). Indeed, when we plot the phase diagram of Fig. 4 with a $h_z = e^{-100}$ a slightly larger value of $\phi_{\text{RLP}}^{\text{min}}$ is obtained as seen in Fig. 4. In the unphysical limit of $h_z \rightarrow 1$ we would obtain a minimum RLP value of $(\phi_{\text{RLP}}^{\text{min}} + \phi_{\text{RCP}})/2$, although as said, this would correspond to an unphysical situation.

However, it should be noted that this argument depends on the assumed exponential form of the density of states. Since at this point we do not have

the exact form for the density of states, the results could change if other more accurate density is found to be valid. On the other hand the prediction of the ground state at RCP, Eq. (21), remains unaffected by the density of state or the value of h_z .

It is interesting to note that we can extend the compactivity to negative values and study the range $X : 0^- \rightarrow -\infty$. Indeed, for any value of h_z , in the limit $X \rightarrow 0^-$ we obtain the lowest volume fraction of the prediction of Eq. (23). Thus, properly speaking, the minimum value of RLP is defined in the limit of negative zero compactivity, and this limit is independent of the value of h_z . The entropy has an interesting behavior in this regime which will be discussed later.

It is important to realize that the region from $X : 0^- \rightarrow \infty$ disappears when $h_z \rightarrow 0$, thus the only meaningful limit is that of $X \rightarrow +\infty$ (which equals both the limits $X \rightarrow -\infty$ and $X \rightarrow 0^-$ when $h_z \rightarrow 0$). Thus, for any practical purpose, Eq. (25) can be considered to be the lowest possible density predicted by the theory. However, notice that the shape of the iso-compactivity curves depends slightly on the value of h_z .

Since we always expect $h_z \ll 1$, it may not be necessary to use the negative compactivity states to describe RLP. We leave this interesting observation for further investigations where the entropy of jamming is treated in more details in [51].

6.1. Volume landscape of jammed matter

Equation (7) plays the role of the Hamiltonian of the jammed system and the jammed configurations can be considered as the minima of (7). Inspired by the physics of glasses and supercooled liquids, we imagine a "volume landscape", analogous to the energy landscape in glasses [64], as a pictorial representation to describe the states of jammed matter. Each mesoscopic jammed state (determined by the positions of the particles, denoted \vec{r}_i , and its corresponding volume w) is depicted as a point in Fig. 5. At the mesoscopic level, the volume landscape has different levels of constant z , analogous to energy levels in Hamiltonian systems.

The lowest volume corresponds to the FCC/HCP structure (with kissing number $z = 12$), as conjectured by Kepler [1]. Other lattice packings, such as the cubic lattice and tetrahedron lattice, have higher volume levels in this representation. Beyond these ordered states, the ensemble of disordered packings is identified within the yellow area in Fig. 5a, corresponding to a system with infinite friction. In this case the partition function is integrated from $z = 4$ to 6, thus all the states are sampled in the configuration average as indicated by the arrow in Fig. 5a. When $X \rightarrow \infty$, all the states are sampled with equal probability, and, when $X \rightarrow 0$, the ground state is the most probable. As the compactivity is varied, the states along the G-line in the phase diagram result. For $\mu \rightarrow \infty$, the maximum volume, $w(z = 4) = \sqrt{3}/2$ is attained for $z = 4$ when $\mu \rightarrow \infty$ in analogy with the high energy states in a classical system.

As we set the friction coefficient to a finite value, the available states in the volume are less, since the integration in the partition function is in the region

$Z(\mu) \leq z \leq 6$. This is indicated in Fig. 5b for a generic $Z(\mu)$. Finally when the friction vanishes, we obtain only the ground state $z = 6$ as indicated in Fig. 5c.

For any value of μ , the lowest state is always at $z = 6$. This corresponds to the states exemplified by the RCP-line in the phase diagram, all of them with a geometrical coordination $z = 6$. Equation (21) indicates that the RCP corresponds to the ground state of disordered jammed matter for a given friction which determines Z , while the RLP states are achieved for higher volume levels as indicated in Fig. 5. An important conclusion is the following: The states along the RCP line all have $z = 6$, independent of Z (and h_z) which ranges from 4 to 6 as a function of the friction coefficient μ . The states along the RLP line all have $z = Z$ (when $h_z \rightarrow 0$). These predictions find good agreement with the numerically generated packings in Section 7.6.

At fixed volume, the jammed states are separated by barriers of deformation energy, as depicted in Fig. 5d. These barriers can be understood as follows: so far we have treated the case of hard spheres considered as soft spheres (interacting via soft-potential such as Hertz-Mindlin forces) in the limit of vanishing deformation or infinite shear modulus. Indeed, the way to consider forces in granular materials is by considering the small tiny deformation at the contact points and a given force law [32]. In a sense, deformable particles are needed when discussing realistic jammed states especially when considering the problem of sound propagation and elastic behavior [65, 66]. In the case of deformable particles the third axis in Fig. 5d corresponds to the energy of deformation or the work done to go from one configuration to the next. This energy is not uniquely defined in terms of the particle coordinates; it depends on the path taken from one jammed state to the next. Thus, we emphasize that the energy in Fig. 5 is path-dependent. The only point where it becomes independent of the path is in the frictionless point. Besides this, the volume landscape in the isostatic plane Figs. 5a-c is well defined and independent of the energy barriers and path dependent issues.

It is important to note that the basins in Fig. 5 are not single states, but represent many microscopic states with different degrees of freedom \vec{r}_i^z , parameterized by a common value of z with a density of states $g(z)$. The basins represent single states only at the mesoscopic level providing a mesoscopic view of the landscape of jammed states. This is an important distinction arising from the fact that the states defined by $w(z) = 2\sqrt{3}/z$, Eq. (7), are coarse grained from the microscopic states defined by the microscopic Voronoi volume Eq. (6) in the mesoscopic calculations leading to (7) as discussed in Jamming I [49]. This fact has important implications for the present predictions which will be discussed in Section 7.5. The advantage of the volume landscape picture is that it allows visualization of the corresponding average over configurations that give rise to the macroscopic observables of the jammed states.

6.2. Equations of state

Further statistical characterization of the jammed structures can be obtained through the calculation of the equations of state in the three-dimensional space (X, ϕ, S) , with S the entropy, as seen in Fig. 6.

The entropy density, $s = \frac{S}{N}$, is obtained as:

$$s(X, Z) = \langle w \rangle / X + \ln \mathcal{Z}_{\text{iso}}(X, Z) \quad (26)$$

This equation is obtained in analogy with equilibrium statistical mechanics and it is analogous to the definition of free energy: $F = E - TS$ where $F = -T \ln \mathcal{Z}$ is the free energy. We replace $T \rightarrow X$, $E \rightarrow \langle w \rangle$. Therefore, $F = E - TS$ or $S = (E - F)/T = E/T + \ln \mathcal{Z}$ is now $s(X, Z) = \langle w \rangle / X + \ln \mathcal{Z}_{\text{iso}}(X, Z)$, which is plotted as the equation of state in Fig. 6.

Each curve in the figure corresponds to a system with a different $Z(\mu)$. The projections $S(X)$ and $S(\phi)$ in Fig. 6 characterize the nature of randomness in the packings. When comparing all the packings, the maximum entropy is at $\phi_{\text{RLP}}^{\text{min}}$ and $X \rightarrow \infty$ while the entropy is minimum for ϕ_{RCP} at $X \rightarrow 0$. Following the G-line in the phase diagram we obtain the entropy for infinitely rough spheres showing a larger entropy for the RLP than the RCP. The same conclusion is obtained for the other packings at finite friction ($4 < Z(\mu) < 6$). We conclude that the RLP states are more disordered than the RCP states. Approaching the frictionless J -point at $Z = 6$ the entropy vanishes. More precisely, it vanishes for a slightly smaller ϕ than ϕ_{RCP} of the order h_z . Strictly speaking, the entropy diverges to $-\infty$ at ϕ_{RCP} as $S \rightarrow \ln X$ for any value of Z , in analogy with the classical equation of state, when we approach RCP to distances smaller than h_z . However, this is an unphysical limit, as it would be like considering distances in phase space smaller than the Planck constant.

It is commonly believed that the RCP limit corresponds to a state with the highest number of configurations and therefore the highest entropy. However, here we show that the states with a higher compactivity have a higher entropy, corresponding to looser packings. Within a statistical mechanics framework of jammed matter, this result is a natural consequence and gives support to such an underlying statistical picture. A more detailed study of the entropy is performed in Jamming III [51].

The interpretation of the RCP as the ground state, $X \rightarrow 0$, with vanishing entropy ($S \rightarrow 0$ and therefore a unique state) warrants an elaboration. We notice that there exist packings above RCP all the way to $\phi_{\text{FCC}} = 0.74048$, but these packings have some degree of order. These partially ordered packings do not appear in our theory because we treat only disordered packings characterized by the mesoscopic volume function which has been derived under the isotropic assumption. By doing so, we explicitly do not consider crystals or partially crystalline packings in the ensemble. This interprets the RCP in the context of the found third-law of thermodynamics. Our approach of neglecting the crystal state from the ensemble has analogies in replica treatment of glasses [67].

The mesoscopic entropy vanishes at RCP. From this point the entropy increases monotonically with X , being maximum for the RLP limit. We note that the microscopic states contribute still to the entropy of RCP giving rise to more states than predicted by the present mesoscopic approach. This case is discussed in more detail in [51].

The equation of state $\phi(X)$ for different values of Z can be seen in the pro-

jection of Fig. 6. The volume fraction diminishes with increasing compactivity according to the theoretical picture of the phase diagram. The curves $\phi(X)$ qualitatively resemble the reversible branch of compaction curves in the experiments of [18] for shaken granular materials and oscillatory compression of grains [20] suggesting a correspondence between X and shaking amplitude. The intention is that, different control parameters in experiments could be related to a state variable, and therefore might help experimentalists to describe results obtained under different protocols.

For any value of Z , there is a common limit $\phi \rightarrow \phi_{\text{RCP}}$ as $X \rightarrow 0$, indicating the constant volume fraction for all the RCP states. The singular nature of the frictionless J -point is revealed as the volume fraction remains constant for any value of X , explaining why this point is the confluence of the isocompactivity lines, including RCP and RLP. We conclude that at the frictionless J -point the compactivity does not play a role, at least at the mesoscopic level.

6.3. Experimental realization of the phase diagram

A reanalysis of the available experimental data tends to agree with the above theoretical predictions. However, it would be desirable to perform more controlled experiments in light of the present results. As in other out of equilibrium systems, such as glasses, the inherent path-dependency of jammed matter materializes in the fact that different packing structures can be realized with different preparation protocols [17, 18, 19, 20, 42] involving tapping, fluidized beds, settling particles at different speeds, acoustic perturbations or pressure waves [9]. Due to this reason, the value of ϕ_{RCP} has not been determined yet for monodisperse frictionless systems. The more extensive evidence for a frictionless RCP appears from simulations, which has been extensively performed for hard and soft sphere systems. They find a common value of RCP for many different preparation protocols [27, 29, 40]. For frictional materials, experiments of Scott and Kilgour [6], and others display a nearly universal value of volume fraction for RCP consistent with the theoretical estimation.

Previous experiments [9] and simulations [32] find that lower volume fractions can be achieved for smaller settling speeds of the grains or slower compression (or quenching) rates during packing preparation. Colloidal glasses find a similar scenario [38, 41], with their glass transition temperature dependence on the quench rate of cooling, although due to different reasons. This raises the question of whether the jamming point is unique or determined by the preparation protocol [41].

The experiments performed by Onoda and Liniger with glass spheres in liquid of varying density to adjust conditions of buoyancy in the limit of vanishing gravity show that for larger values of gravity, the volume fraction decreases. This indicates that settling speed of the particles can determine the final volume fraction. Indeed, it was found numerically that the compression rate during preparation of the packings is a systematic way to obtain lower packing fractions, such that lower volume fractions can be achieved with quasi-static compression rates during preparation of the packings [32].

On the other hand, measuring the mechanical coordination number in experiments seems to be an even more difficult task. In the phase diagram, the RCP can be found at the frictionless point with the highest possible coordination number $Z = 6$. Such a value of Z has been observed in the experiments of Brujić *et al.* on concentrated emulsions near the jamming transition [63] and simulations of droplets.

The experiments of Bernal [4] simultaneously measured the coordination number and the volume fraction. Indeed, Mason, a postgraduate student of Bernal, took on the task of shaking glass balls in a sack and freezing the packing by pouring wax over the whole system. He would then carefully take the packing apart, ball by ball, painstakingly recording the positions of contacts for each of over 8000 particles [4]. Their result is a coordination number $Z \approx 6$ and a volume fraction $\phi \approx 0.64$ which corresponds to the prediction of the frictionless point in the phase diagram. This may indicate that the particles used in the experiment of Bernal have a low friction coefficient.

Another explanation, more plausible, is that the coordination number measured by Bernal is not the mechanical one, but the geometrical one. Indeed, we may argue that the only coordination that can be measured in experiments of counting balls 'a la Bernal' is the geometrical one, since, one is never sure if the contacting balls were carrying a force or not. Bernal could only measure geometries, not forces. This is in addition to the uncertainty in the determination of the contacts with such a rudimentary method as pouring wax and then counting one by one the area of contact. The theory predicts that along the RCP-line, all the RCP states have geometrical $z = 6$, while Z ranges from 4 to 6. Thus, it is quite plausible that the coordination number in Bernal experiments is the geometrical one, $z = 6$, in agreement with the theory.

It is worth noting that since the labor-intensive method patented half a century ago by Bernal, other groups have extracted data at the level of the constituent particles using X-ray tomography [46]. Such experiments may give a clue to the relationship between coordination number and volume fraction. The experimental data, to date, seems in good agreement with the present theory. However, this method does not directly determine the contacts to verify whether the particles are touching or just very close together. Furthermore, the method cannot measure forces so the distinction between geometrical and mechanical coordination is not possible to achieve in this experiment.

An answer might be obtained using methods from biochemistry being developed at the moment [68]. These methods promise to provide the high resolution to determine the contact network with accuracy to develop an experimental understanding of the problem.

An alternate way might be generating the packings in the phase space through numerical simulations, where both volume fraction and coordination number could be easily determined. Since Z is directly determined by μ , and the compactivity determines what value of the volume fraction a packing has between the limits of the phase diagram, the main question is how to generate packings with different ϕ for a fixed μ to allow the exploration of the phase diagram.

7. Numerical tests

In this section we perform two different numerical tests: on the predictions of the theory and the assumptions of the theory. The former are explained in Section 7.3 while the latter are elaborated in Section 7.6. It is worth mentioning that while the predictions can be tested with packings prepared numerically and experimentally, the test of the assumptions of the theory is not so trivial. This is because the theory is based on the existence of quasiparticles which carry the information at a mesoscopic scale. Thus, in principle we cannot use real packings, such as computer generated packings or experimental ones, to measure the quasiparticles. The information obtained from those packings already contains ensemble averages through the Boltzmann distribution and density of states. That is, it is in principle not possible to isolate the behavior of quasiparticles from the real measures rendering difficult to properly test some of the assumptions of the theory at the more basic mesoscopic scale. In Section 7.6 we attempt to perform such a test, especially since we can easily obtain the packings at the RLP line or the infinite compactivity limit. These packings are fully random obtained as flat averages in the ensemble without the corresponding Boltzmann factor and may contain direct information on the mesoscopic fluctuations.

The existence of the theoretically inferred jammed states opens such predictions to experimental and computational investigation. We numerically test the predictions of the phase diagram by preparing monodisperse packings of Hertz-Mindlin [35, 36] spheres with friction coefficient μ at the jamming transition using methods previously developed [27, 32, 65, 66].

We test the theoretical predictions and show how to dynamically generate all the packings in the phase space of configurations through different preparation protocols. Although diverse states are predicted by the theory, they may not be easily accessible by experimentation due to their low probability of occurrence. For instance, we will find that the packings close to the C-point (high volume fraction, high friction, low coordination) are the most difficult to obtain.

The advantage of our theoretical framework is that it systematically classifies the different packings into a coherent picture of the phase diagram. In the following we use different preparation protocols to generate all the phase space of jamming. In particular we provide a scheme to reproduce the RCP and RLP-lines amenable to experimental tests.

We achieve different packing states by compressing a system from an initial volume fraction ϕ_i with a compression rate Γ in a medium of viscosity (damping) η where the particles are dispersed. The system is defined by the friction coefficient μ which sets $Z(\mu)$ according to Fig. 2. While the simulations are not realistic (no gravity, boundaries, or realistic protocol is employed), they provide a way to test the main predictions of the theory. The final state (ϕ, Z) is achieved by the system for every $(\phi_i, \Gamma, \eta, \mu)$ at the jamming transition of vanishing stress with a method explained next.

It should be noted that other experimental protocols could be also adapted to the exploration of the phase diagram, including (a) Gentle tapping with servo mechanisms that adjust the system at a specified pressure [66], (b) Gentle

tapping with external oscillatory perturbations, (c) Settling of grains under gravity in a variety of liquids with viscosity η , (d) fluidized beds.

Relation with hard sphere simulations.— The present algorithm finds analogies with recent attempts to describe jamming using ideas coming from the theory of mean-field spin glasses and optimization problems [38, 41]. This is an interesting situation since it has been shown that in the case of hard spheres the system always crystallizes unless an infinite quench is applied [10].

However, our soft sphere simulations do not produce appreciable crystallization in the packing. This situation can be understood as following: In order to avoid the (partial) crystallization in practice, a fast compression is needed. A simple dimensionality analysis tells that the quenching rate $\Gamma \propto G^{1/2}$, where G is the shear modulus of the grains (see Fig. 7). This analysis allows for comparison of our soft ball simulations with the hard sphere simulations used in other studies [10]. One could imagine that there exists a typical quench rate, depending on the stiffness of the grains, as a division of the ordered and disordered (jammed) phases. It is interesting to note that at the hard-sphere limit, $G \rightarrow \infty$, all the packings are in the ordered phase except when $\Gamma \rightarrow \infty$, where $\phi \approx 0.64$. This explains the behavior of the hard sphere packings found in previous works [10]. For the soft ball case, the situation is more subtle since a certain range of compression rate is acceptable for the acquirement of disordered packings. It is in this range that we perform simulations. However, it should be noted that the above simple dimensionality analysis does not consider the dependence on dimensions and algorithms, which probably has important effects in the real situation.

According to this picture, in the theoretical limit of infinitely slow quench rates, the system should in principle crystallize for any G . However in practice, this limit is almost impossible to achieve experimentally. For sufficiently fast quench rates, crystallization can be avoided and a granular system is stuck in a random jammed configuration since its configurational relaxation time exceeds the laboratory timescale. The contention is that, for a well defined set of quenches, the system does not crystallize and the study of the disordered phase ensues. Indeed, numerical and experimental evidence points to the validity of this assertion. The present theory neglects the existence of the ordered phase and assumes an ensemble of the disordered states. A more general theory will account for the ordered states as well. But this is a very difficult problem in jamming: a full theory that accounts for RCP and crystallization. A recent study has attempted to answer the question using Edwards' thermodynamic viewpoint of granular matter [69]. From the simulation point of view, we can say that our soft sphere approach does not produce crystallization while the hard sphere approach does not produce randomness for any finite compression rate.

7.1. Molecular dynamics simulations of grains

We prepare static packings of spherical grains interacting via elastic forces and Coulomb friction (see [27, 32] for more details). The system size ranges from $N = 1,024$ to $N = 10,000$ particles. Two spherical grains in contact at

positions \vec{x}_1 and \vec{x}_2 and with radius R interact with a Hertz normal repulsive force [35]

$$F_n = \frac{2}{3} k_n R^{1/2} \delta^{3/2}, \quad (27)$$

and an incremental Mindlin tangential force [36]

$$\Delta F_t = k_t (R\delta)^{1/2} \Delta s, \quad (28)$$

Here the normal overlap is $\delta = (1/2)[2R - |\vec{x}_1 - \vec{x}_2|] > 0$. The normal force acts only in compression, $F_n = 0$ when $\delta < 0$. The variable s is defined such that the relative shear displacement between the two grain centers is $2s$. The prefactors $k_n = 4G/(1-\nu)$ and $k_t = 8G/(2-\nu)$ are defined in terms of the shear modulus G and the Poisson's ratio ν of the material from which the grains are made. We use $G = 29$ GPa and $\nu = 0.2$ typical values for spherical glass beads and we use $R = 5 \times 10^{-3}$ m and the density of the particles, $\rho = 2 \times 10^3$ kg/m³. Viscous dissipative forces are added at the global level affecting the total velocity of each particle through a term $-\gamma\dot{\vec{x}}$ in the equation of motion, where γ is the damping coefficient related to the viscosity of the medium $\eta = \gamma/(6\pi R)$. Sliding friction is also considered:

$$F_t \leq \mu F_n. \quad (29)$$

That is, when F_t exceeds the Coulomb threshold, μF_n , the grains slide and $F_t = \mu F_n$, where μ is the static friction coefficient between the spheres. We measure the time in units of $t_0 = R\sqrt{\rho/G}$, the compression rate in units of $\Gamma_0 = 5.9t_0^{-1}$ and the viscosity in units of $\eta_0 = 8.2R^2\rho/t_0$. We choose the time step to be a fraction of the time unit t_0 , which is the time that it takes for sound waves to propagate on one grain (see [66] for more details). The dynamics follows integration of Newton's equation for translations and rotations.

7.2. Preparation protocol: Packings at the jamming transition with the split algorithm

The critical volume fraction at the jamming transition, ϕ_c will be identified by the ‘‘split’’ algorithm as explained in [32], allowing one to obtain packings at the critical density of jamming with arbitrary precision. Preliminary results indicate that lower values of ϕ are obtained for slow compression [32]. Thus we expect that by varying Γ or η the phase space will be explored. Also, the initial ϕ_i plays an important role in achieving packings close to the RCP line.

The preparation protocol consists of first preparing a gas of non-interacting particles at an initial volume fraction ϕ_i in a periodically repeated cubic box. The particles do not interact and therefore the stress in the system is $\sigma = 0$ and $Z = 0$.

To generate a random configuration with friction at volume fraction ~ 0.64 is very difficult. Therefore to achieve any volume fraction in this initial stage, we initially work with a frictionless system. We first generate a very dilute (un-jammed gas of non interacting particles) grain configuration randomly, usually with a volume fraction $\phi_0 \approx 0.30 \sim 0.36$. Then we apply an extremely slow

isotropic compression without friction on this dilute configuration until the system reaches another unjammed configuration at higher density, ϕ_i (see Fig. 8a). The reason to add an extremely slow isotropic compression to the dilute configuration is to avoid involving any kinetic energy to keep the system as random as possible. After obtaining this unjammed state with initial volume fraction ϕ_i , we restore friction and a compression is applied with a compression rate Γ until a given volume fraction ϕ_1 . Then the compression is stopped and the system is allowed to relax to mechanical equilibrium by following Newton's equations without further compression.

After the compression, two things can occur (see Fig. 9):

(a) The system jams: If the volume fraction ϕ_1 is above the jamming point, $\phi_1 > \phi_c$, then the stress will decrease and ultimately stabilize to a finite nonzero value, meaning that the pressure of the system remains unchanged (usually $\Delta\sigma < 10^{-3}$ Pa, red line, Fig 9) over a large period of time (usually $\sim 10^7$ MD steps). The coordination number usually has a first initial decrease, but if the system is jammed it will also stabilize at a constant value above the isostatic minimal number (inset Fig. 9).

(b) The system is not jammed: If the volume fraction ϕ_2 is below the jamming point, $\phi_2 < \phi_c$, then the stress and the coordination number will relax to zero. This fact is illustrated in Fig. 9. If the packing has $\phi_1 > \phi_c$, it stabilizes at a non-zero pressure above the jamming transition, but the pressure decreases very quickly to zero (the system is not jammed) if $\phi_2 < \phi_c$, even though ϕ_1 and ϕ_2 differ only by 2×10^{-4} .

We identify the exact volume fraction of the jamming transition ϕ_c , as follows [32]: A search procedure consisting of several cycles is applied such that in each cycle we fix the lower and upper boundaries of ϕ_c , see Fig. 10. The difference between the boundaries gets smaller as the cycles proceed, meaning that ϕ_c is fixed with higher and higher precision. We start from the packing of high volume fraction $\phi_1 > \phi_c$ and generate a series of packings with step-decreasing volume fractions until the first packing with zero pressure is observed, which has a volume fraction $\phi_2 = \phi_1 - \Delta\phi$, where $\Delta\phi$ is the difference between the jammed packing fraction ϕ_1 and the unjammed packing fraction ϕ_2 . Thus, ϕ_c is bounded between $\phi_1 - \Delta\phi$ and ϕ_1 . Then we test $\phi = \phi_1 - \Delta\phi/2$. If $\phi = \phi_1 - \Delta\phi/2$ is stable, ϕ_c is between $\phi_1 - \Delta\phi$ and $\phi_1 - \Delta\phi/2$. If $\phi = \phi_1 - \Delta\phi/2$ is unstable, ϕ_c is between $\phi_1 - \Delta\phi/2$ and ϕ_1 . Therefore, in this cycle, we reduce the region where ϕ_c possibly lies in from $\Delta\phi$ to $\Delta\phi/2$. If we carry out this cycle for n times, we improve the precision to $\Delta\phi_n = \Delta\phi/2^n$. In our simulations cycling ceases when $\Delta\phi_n$ gets below 2×10^{-4} and $n = 12$. A similar algorithm was employed in [32] to study the approach to the jamming transition by preparing packings at a finite pressure. In the present work we are interested in jammed packings at vanishing pressure, right at the jamming transition in the isostatic plane defined for all friction coefficients.

It is important to determine whether the packings are jammed in the sense that they are not only mechanically stable but also they are stable under perturbations. Our numerical protocols assure that the system is at least locally jammed since each particle is in mechanical equilibrium [62]. To test if the

system is collectively jammed is more involved. For frictionless systems, where tangential forces are removed, we use the Hertz energy $U_{\text{hertz}} = \frac{4}{15} k_n R^{1/2} \delta^{5/2}$ to test whether the Hessian of the jammed configurations is positive [29]. We find that the frictionless configurations have positive Hessian indicating that they are collectively jammed. However, this method is not useful when considering frictional systems. The energy of deformation depends on the path taken to deform the system and cannot be defined uniquely. In this case, a numerical test of the stability of the packings applies a small random velocity to each jammed particle. We find that the packings are stable to small perturbations consisting of external forces of the order of 0.1 times the value of the average force, indicating that the packings may be collectively jammed.

To test for more strict jammed conditions involves studying the stability under boundary deformations. We have tested that our packings are stable under the most common strain deformations to isotropic packings by performing a uniaxial compression test, a simple shear and a pure shear test.

A simple shear test implies a strain deformation $\Delta\epsilon_{12} = \Delta\epsilon_{21} \neq 0$, while the rest of the strain components ϵ_{ij} remain constant. A pure shear test is done with $\Delta\epsilon_{11} = -\Delta\epsilon_{22} \neq 0$ and a uniaxial compression test along the 1-direction is performed by keeping the strain constant in $\Delta\epsilon_{22} = \Delta\epsilon_{33} = 0$, and $\Delta\epsilon_{11} \neq 0$. Here, the strain ϵ_{ij} , is determined from the imposed dimensions of the unit cell. For example, $\epsilon_{11} = \Delta L/L_0$ where ΔL is the infinitesimal change in the 11 direction and L_0 is the size of the reference state.

In all cases the packings are stable under strain perturbations indicative of the existence of a finite shear modulus (from the shear and compression tests) and a finite bulk modulus (from the compression test) of the jammed packings. A full investigation of the elasticity of the jamming phase diagram is left for future studies. It suffices to state that the numerically found states can be considered to be mechanically stable jammed states amenable to a statistical mechanical description in the sense of the reversible branch of compaction in the experiments of [18, 20, 42].

7.3. Results: phase diagram

We repeat the above procedure 10 times with different random initial configurations to get a better average of ϕ_c . Figure 11 shows the results for a system of $N = 1024$. All of the packings shown in the present work as well as the code to generate them are available at <http://jamlab.org>. Each data point corresponds to a single set of $(\phi_i, \Gamma, \eta, \mu)$ and is averaged over these 10 realizations. We consider $0.40 \leq \phi_i \leq 0.63$, $10^{-7} \leq \Gamma \leq 10^{-3}$, $10^{-4} \leq \eta \leq 10^{-3}$, and $0 \leq \mu \leq \infty$. The error of ϕ_c obtained over the 10 realizations as shown in Fig. 11 is usually 5×10^{-4} , larger than the precision of the split algorithm (2×10^{-4}). In general, all numerically generated jammed states lie approximately within the predicted bounds of the phase diagram.

The plot in Fig. 11a explores the dependence of the packings (ϕ, Z) on the initial state ϕ_i . (In the plot, ϕ refers to the ϕ_c obtained in a split algorithm). In Fig. 11 we plot our results for a fixed quench rate $\Gamma = 10^{-7}$ and damping coefficient $\eta = 10^{-3}$ (except for the last orange curve on the right with $\eta =$

10^{-4}) and for different initial states ranging from left to right (see Fig. 11 for details) Each color here corresponds to a particular ϕ_i (0.40 at the left to 0.63 at the right), while each data point along a curve corresponds to a system prepared at a different friction from $\mu = 0$ at $Z \approx 6$ to $\mu \rightarrow \infty$ at $Z \approx 4$. For instance, the states joined by the dashed lines in Fig. 11a are for systems with the same μ . While these lines are approximately horizontal, indicating an approximate independence of Z on the preparation protocol ϕ_i , we observe deviations specially around the RLP line for intermediate values of μ . Despite this, the $Z(\mu)$ dependence is approximately valid as seen in Fig. 2, which is plotted using the results of Fig. 11a.

We find that the packings prepared from the larger initial densities ϕ_i closely reproduce the RCP line of zero compactivity at ϕ_{RCP} , confirming the prediction that RCP extend along the vertical line from the J-point to the C-point.

We find that the packings along the RCP line have equal geometrical coordination number $z \approx 6$ but differ in their mechanical one from $Z = 6$ to $Z \approx 4$, in agreement with theory (see Section 7.6). These states are then identified with the ground state of jammed matter for a given μ as depicted in the volume landscape picture of Fig. 5.

In the limit of small initial densities (see curves for $\phi_i = 0.40, 0.53$ and 0.55 in Fig. 11a) we reproduce approximately the predictions of the RLP-line. These packings follow the theoretical prediction for infinite compactivity except for deviations (less than 5%) in the coordination number for packings close to the lower value of $Z = 4$, where the numerical curve seems to flatten out deviating from the theory. Numerically, we find the lowest volume fraction at $\phi_{\text{RLP}}^{\text{min}} = 0.539 \pm 0.003$, close to the theoretical prediction, $\phi_{\text{RLP}}^{\text{min}} = 0.536$. We notice that the theoretical lines in Fig. 11 are obtained for $h_z = e^{-100}$, thus the minimum RLP deviates slightly from the theoretical prediction in the limit $h_z \rightarrow 0$ as discussed in Section 6.

Packings with the lowest Z correspond to infinitely rough spheres. The deviation of coordination number between theory and simulation (specially at low volume fraction) could be from the system not achieving an isostatic state at infinite friction. We were not able to generate packings with exactly $Z = 4$ but our algorithm generates packings very close to this isostatic packings at $Z \approx 4.2$ for $\mu = 10^4$. In general, we find that while there are many states along the RLP line, the barriers of these states decrease as the coordination number decreases towards $Z = 4$, i.e. when the friction increases. Thus, the states at the lower left part of the phase diagram are very difficult to equilibrate.

Besides the states delimiting the phase space, we generate other packings with intermediate values of $\phi_i = 0.57, 0.59, 0.61$ as shown in Fig. 11a. Interestingly, we find that these states (all obtained for fixed $\Gamma = 10^{-7}$ and $\eta = 10^{-3}$) closely follow the predicted lines of isocompactivity as indicated in the figure. We find that the simulations from $\phi_i = 0.57, 0.59, 0.61$ correspond to compactivities $X = 1.62, 1.38, \text{ and } 1.16$, respectively (measured in units of $10^{-3}V_g$).

The constant h_z weakly affects the finite compactivity lines. We find that $h_z = e^{-100}$ provides the best fit to the data for finite isocompactivity lines in Fig. 11a. Thus, with reasonable approximation and for this particular protocol,

we identify the density of the initial state, ϕ_i with the compactivity of the packing, providing a way to prepare a packing with a desired compactivity. We note, however, that other values of h_z produce approximately the same phase diagram boundaries (i.e., the RLP and RCP lines, as long as $h_z \ll 1$) but do not fit the isocompactivity lines within as accurately. Thus, the identification of the compactivity with ϕ_i remains dependent on this particular value of h_z used to fit the theory.

We also test the dependence on the state of the packings with the compression rate Γ and viscosity η . Both parameters should have similar effects since they slow down the dynamics of the grains. Figures 8b and 8c represent typical preparations. In general, we reproduce the RLP line for slow quenches or for large viscosities as seen in Fig. 11b (for $\phi_i = 0.40$ in black). In this case, the grains are allowed to slide and develop large transverse displacements and Mindlin forces with the concomitant low ϕ and large compactivity. Therefore we find a predominance of the Mindlin forces over the normal Hertzian forces as a characteristic of the lower volume fractions of RLP, having a pronounced path dependent structure with large compactivity in the packing. When the compression rate is increased or the damping is reduced we find packings with higher volume fractions as indicated in Fig. 11b. Indeed, analogous protocol to generate these packings would be to change the damping coefficient by immersing the particles in liquids of different viscosities.

It is also interesting to investigate the packings generated by fixed friction and varying quenched rate, since this situation corresponds to a given system. For a given μ we find approximately a common value of $Z(\mu)$ independent of Γ and ϕ_i , as discussed in Fig. 2, indicating that the curve $Z(\mu)$ is roughly independent of the protocol. Thus, a fixed μ corresponds to a horizontal line in the phase diagram as indicated in Fig 11a by the dashed lines.

Figure 8 shows a summary of the numerical protocols we use to generate the packings in the phase diagram. The “easiest” packings to generate are along the RLP line (Fig. 8b, c) while the most difficult are deep in the phase diagram with low coordination number (large friction) and high volume fraction, that is near the C-point (Fig. 8a). In general, we always start with a dilute unjammed (non-interacting gas) sample without friction and compressed slowly until another dilute sample not jammed at a volume fraction ϕ_i . If ϕ_i is around or smaller than 0.55 then the RLP line is obtained. If we decrease by 3 orders of magnitudes the compression rate using this initial density, we move inside the phase diagram, though not substantially, as indicated schematically in the figure.

Therefore, in order to access the inner states around the C-point at high friction, we took another route. We prepared a frictionless dilute unjammed sample at a higher ϕ_i , which can be as close as possible to ~ 0.63 since frictionless spheres only jam at RCP. Then we switched on friction and got the packings inside the phase diagram as indicated in Fig. 8a. We realize that switching on and off friction is impossible in experiments. However, a possible way to experimentally realize the path to the C-point is by resetting the path dependency to zero along the preparation protocol: this path could be reproduced by stabi-

lizing a frictional packing with fast compressions and resetting the interparticle forces by gently tapping. This will simulate the lost of path dependence that we simulate by the initial compression without friction and may allow to reach the packings around the C-point.

7.4. Compactimeter for granular matter and the ABC experiment

At this point we do not have a theoretical explanation for why packings with the same initial unjammed state ϕ_i end up having the same compactivity when jammed after compression. It is important to note that this finding is based on the particular value we use for h_z , such that a change in h_z gives rise to different lines of isocompactivity which may not fit the simulation results of Fig. 11a so closely. Nevertheless, the close fit between theory and simulation deserves an explanation.

We may conjecture that ϕ_i determines a type of disorder quenched in the initial configuration that leads to systems with the same compactivity but different volume fractions and coordination numbers, evidenced by our results. We can use this empirical result to control the compactivity of the packing, at least for this particular protocol, defining a “granular compactimeter”. Laboratory measurements of compactivity usually involve indirect measures through Fluctuation-Dissipation relations between fluctuations and response functions [18, 19, 24]. However, there is no simple thermometer (or “compactimeter”) to measure this observable directly in a packing. Furthermore, there is no simple way to prepare a packing with a desired compactivity. Our results can be used to, at a minimum, define packings with equal compactivity. The empirical identification of X with ϕ_i promotes the possibility of controlling X within this particular protocol, an important step in any thermodynamical analysis.

The advance of a granular thermodynamics crucially depends on the invention of a thermometer that can easily measure the compactivity, as in Fig. 12. A zero-th law of thermodynamics presents serious challenges in granular materials since there is no straight forward way to define a compactivity bath or reservoir.

The present theory predicts the dependence of the volume fraction, $\phi(X)$, on the compactivity, allowing for the development of a compactimeter: Such a device consists of a known granular medium, having a given μ and, therefore, a given coordination number. The compactimeter is inserted in a granular system and both, system and compactimeter, are gently shaken to allow for equilibration at a common compactivity (the compactimeter has a flexible membrane that allows volume transfer between both systems in contact). The volume of the grain in the compactimeter will adjust accordingly and the compactivity can be read directly from the scale attached to it through the equation of state, $X(\phi)$, provided by the theory.

The foundation of the above compactimeter relies on the validity of a zero-th law for granular thermodynamics that determines the equilibration at a given compactivity of a system: Two systems in contact should mechanically equilibrate at the same compactivity. A recent experiment [70] found a materials-independent relationship between the average volume fraction and its fluctua-

tions in two equilibrated granular subsystems, which gives support to the zero-th law. Further test of the zero-th law is difficult to facilitate without theoretical guidance. Thus, it will be useful to perform the following test, either numerically or experimentally to test not only the idea of equilibration but also the possibility to describe granular matter under the V-ensemble. Such a test has been labeled the ABC experiment as proposed by Edwards [45], which is now possible to perform using the phase diagram.

Two packings are numerically prepared at points A and B in the Fig. 13 for different μ , $\mu_A < \mu_B$. The systems are equilibrated at different compactivities $X_A < X_B$ by using different ϕ_i . They are then put into contact through a flexible membrane (or by simply putting the particles at the surface in contact) and allowed to mechanically equilibrate by gently shaking the system. Numerically, this can be simulated with the same compression methods as explained in Section 7. The total volume is kept fixed and the volumes of the subsystems should change accordingly, $V = V_A + V_B$. If the AB system equilibrates at the same compactivity, then it will follow the trajectory depicted in Fig. 13 towards the state C of equilibration along the isocompactivity line. There is no need to measure the compactivity of the final packing. By just measuring the final volumes V_A and V_B (or their volume fractions) will suffice. This will provide an important test for the V-ensemble and compactivity to describe jammed matter, as well as the validity of the phase diagram.

Another intriguing possibility would be to mix a frictionless A packing at the J-point with an infinite friction B packing at the L-point, which can be achieved numerically. This AB system would provide the maximum difference between the isolated packings, allowing study of the zero-th law with more accuracy. According to theory, the frictionless packing is independent of X . Therefore, it should remain at the J-point. The $\mu \rightarrow \infty$ packing should, in principle, equilibrate at any X or volume fraction along the G-line. Most probably, it would stay put at the L-point since the A and B packings are joined by the isocompactivity $X \rightarrow \infty$ line already. In any case, the resulting AB packing should fall inside the phase diagram if the theory is correct. If it does not equilibrate (falling outside the phase diagram, we note that the two packings are at the borderline), it could indicate the breakdown of the approach. Two conclusions could be reached from the failure of such a test. Either the V-ensemble is wrong or the approximations of the V-ensemble theory are not correct. In the latter, more sophisticated theories should be developed. If the former case occurs, then a different ensemble will have to be considered beyond isostaticity.

7.5. Microscopic states versus mesoscopic states

The notion that RCP arises for $X = 0$, implying that there are no fluctuations at RCP, deserves some discussion. Furthermore, it is important to discuss the implications of the related coincidence of RCP and RLP at the frictionless point. That is, the fact that for frictionless particles there is a unique state of jamming and therefore the compactivity is irrelevant when $\mu = 0$.

First of all, we need to emphasize that these results should be interpreted at the mesoscopic level. Thus, there is one mesoscopic state at RCP and only the mesoscopic entropy vanishes at this point. These results provides an unambiguous interpretation of RCP only at the meso level. As discussed above, for a single mesoscopic state, there are many microscopic states average out in the calculation of the average free volume function $w(z)$ which is used in the partition function Eq. (19) (see also Jamming I [49]). Therefore, we expect that these microscopic states will contribute to the entropy of RCP (see Jamming III [51] for a discussion) as well as giving rise to other states perhaps with different volume fraction. Below we elaborate on the existence of microscopic and mesoscopic packing states. This point is better discussed in terms of the volume landscape of Fig. 5: all the jammed states are degenerated around the mesoscopic ground state with the coordination number $z = 6$. These states have slightly different volume fractions, leading to microscopic fluctuations which are coarse-grained in the mesoscopic theory.

The existence of microscopic states neglected at the mesoscopic level raises an interesting analogy with recent work of Zamponi and Parisi [38] where the jammed states are considered as infinite pressure glassy states obtained after a fast compression from a liquid state at finite temperature. They propose that a range of different volume fractions of jamming can be achieved according to the initial state from where the quench is started, with the maximum possible jammed density obtained when the initial density is the Kauzmann point of the ideal glass. In their representation (see Fig. 4 in [38]) a range of initial densities in the liquid phase $\varphi \in [\varphi_d, \varphi_K]$, where φ_d is the density where many metastable states first appear in the liquid phase as suggested by mean field model picture of the glass transition, and φ_K is the Kauzmann density of the ideal glass transition, gives rise to a final density of jamming, $\varphi_j(\varphi)$, obtained after a fast quench from φ . Two limiting densities of jamming are predicted: the minimum at $\varphi_j(\varphi_d) = \varphi_{th}$ and the maximum volume fraction obtained after a quench from the Kauzmann point, $\varphi_j(\varphi_K) = \varphi_0$.

This situation could be interpreted in term of neglecting the microscopic states in our theory. It is also a question whether the states at infinite pressure obtained using fast quenches from a liquid state “a la Zamponi” are equivalent to the jammed state obtained in our approach for soft spheres. Our volume ensemble approach might differ from the energy/force ensemble used in the work of Zamponi-Parisi. Further investigations are required to reveal the possible differences.

7.6. Geometrical versus mechanical coordination number: measuring the behavior of quasiparticles

In Section 7.3 we have tested the predictions of the theory. In this Section we attempt to test some of the assumptions of the theory, specially those related to the quasiparticles of $w(z)$ and the bounds in z and its distribution. A quasiparticle is a mathematical entity that is, in principle, impossible to isolate from the structure of a real packing prepared either with MD computer simulations or experiments, rendering the measurement of their properties from real

packings difficult. This is because real packings already contain the ensemble average, and we can not dissociate the ensemble, with the Boltzmann distribution of states, compactivity and density of states, from the isolated statistics of a quasiparticle.

Quasiparticles can be tested by preparing random packings with prescribed geometrical coordination number. However, below, we argue that we may obtain approximate properties from real packings in the limit $X \rightarrow \infty$ and $h_z \rightarrow 0$ based on the following observations: First, when $X \rightarrow \infty$ the Boltzmann factor is one, and the average in the partition function is flat over the configurations up to the density of states. Furthermore, the density of states is found to be a very fast decaying function of z . These two results implies that along the RLP-line of real packings (either numerical or experimental) we can obtain fully random packings which could reveal the properties of the quasiparticles. Under this approximation we can then test some of the approximations of the theory. However, the conclusions from this section remain approximate.

We have proposed that the bounds of the geometrical coordination number are $Z \leq z \leq 6$ and below we test these bounds. We find numerically that the quasiparticles size is of the order of two particle diameters. Once z is averaged over this range, we find that z ranges approximately between $(Z, 6)$. In fact, we find even more narrow distribution than theoretically expected. This is due to the fact that we define z without the microscopic fluctuations but including the mesoscopic fluctuations. Once we average over its neighbors, we not only remove the microscopic fluctuations but also, partially, the mesoscopic ones. In the limiting case of no mesoscopic fluctuations, when $X = 0$ along the RCP line, we find a very narrow distribution at $z \approx 6$ for any value of Z and μ , after averaging z over a mesoscopic region of two particle diameters. The distribution is even narrower when z is coarse-grained over a region of four particle diameters.

The X-ray tomography experiments of Aste [46] (Fig. 6a) reveal the trend predicted by Eq. (7) between the inverse of the Voronoi volume and the number of neighbors of a set of Voronoi cells with similar volumes. However, it is evident from the figure that such number of neighbors is spanning a range of values between ~ 4 and ~ 10 . The reason why the Aste's group [46] found a wider range of z is possibly due to the fact they did not consider a range of coarse-graining.

A question arise as how to identify the geometrical from the mechanical coordination number, even numerically. A detailed discussion of this topic appears in Ref. [71]. Below we summarize the results. Strictly speaking, this distinction is not possible to materialize in real packings. Again, we need to generate random packings from a geometrical point of view, without resorting to forces, and then study their distribution in real packings where forces are taken into account. Nevertheless, we follow the following approximate scheme to try to obtain information of the quasiparticles from real packings.

Even in numerical simulations, there is always a round off error associated to measurements. Thus, two particles that may not be in contact (giving rise to a zero force) may be close enough to be considered as contributing to the geometrical coordination. Indeed, it is known that $g(r)$ has a singularity [72],

$g(r) \sim (r - .5)^{-0.5}$, implying that there are many particles almost touching. Following this consideration, we introduce a modified radial distribution function (RDF) $g_z(r)$ in order to approximately identify z and Z from real packings:

$$g_z(r) = \frac{1}{N} \frac{R^2}{r^2} \sum_i^N \sum_{j \neq i}^N \Theta\left(\frac{r_{ij}}{r-R} - 1\right) \Theta\left(\frac{r+R}{r_{ij}} - 1\right), \quad r > R \quad (30)$$

where R is the radius of particle, N is the number of particles, r_{ij} is the distance of two particle's centers, $r_{ij} = |\vec{r}_i - \vec{r}_j|$, and Θ is the Heaviside step function. The RDF describes the average value of the number of grains in contact with a virtual particle of radius r , and the factor of R^2/r^2 is the ratio of a real sphere's area and the virtual one's.

$g_z(r)$ measures the number of balls with their volume intersecting the surface of a sphere of radius r measured from the center of a given ball. When $r = R$ in (30) we obtain the mechanical coordination number while the geometrical one is obtained for a small value $\Delta r = \frac{r-R}{2R} \neq 0$ for which we distinctly find a signature from computer simulations, unambiguously defining it at $\Delta r = 0.04$.

Figures 14 and 15 plot the $g_z(\Delta r)$ of packings with various friction coefficient μ on the isostatic plane along the RCP and RLP lines respectively. Following the definition of Eq. (30), g_z , with $\Delta r = 0$, should be directly equal to the mechanical coordination number, Z , and should range from 4 to 6 along both RCP and RLP (if $h_z \ll 1$) lines which is confirmed by our numerical simulations in Figs. 14 and 15, respectively.

Furthermore, as shown in the figures, we find that $g_z(\Delta r)$ along the RCP line, increases slightly as Δr increases, and finally reach the same value of g_z at $\Delta r = 0.04$ as shown in Fig. 14. We identify the geometrical coordination number as $z = g_z(0.04)$ under the accuracy of the simulations. Therefore, we conclude that all RCP states have approximately the same geometrical coordination number, $z \approx 6$, in agreement with the theory. In terms of the volume landscape of Fig. 5, the states along the RCP line are ground states with different friction at $X = 0$. Thus they should all have $z = 6$. We notice that $g_z(\Delta r = 0.04) = 6.65 > 6$, which may result, firstly, from the approximate nature of our measurements of z from real packings since we are not measuring the quasiparticles directly, and, secondly, from the increasing of the coordination number slightly away from the critical point as the local volume fraction ϕ increases slightly as $Z - Z_c \sim (\phi - \phi_c)^\beta$. We note that Z is also slightly increased from the isostatic point.

Along the RLP line, Fig. 15, we find that the geometrical coordination number as extracted from $g_z(0.04)$ is very close to the mechanical one. Since the RLP line is at $X \rightarrow \infty$ and $h_z \ll 1$, all the states along RLP have $z \approx Z$ as we move along the line varying the friction coefficient. Thus, the numerical results confirm the theory, and further confirm that the value of h_z is very small.

Next, we study the coarse-grained coordination number $\langle z \rangle_l$ as defined as,

$$\langle z \rangle_l = \frac{1}{N_l} \frac{R^2}{r^2} \sum_i^{N_l} \sum_{j \neq i}^{N_l} \Theta\left(\frac{r_{ij}}{r-R} - 1\right) \Theta\left(\frac{r+R}{r_{ij}} - 1\right), \quad r > R \quad (31)$$

where N_l is the number of the particles inside a coarse-grained spherical range with a radius of l . Figures 16 and 17 plot the PDF of $\langle z \rangle_l$ for all the packings along the RCP and RLP lines, respectively. The distributions show a narrow shape, and the average value gives the value of $g_z(r)$, i.e.,

$$\overline{\langle z \rangle_l} = g_z(r). \quad (32)$$

We find that all the $P(\langle z \rangle_l)$ along the RCP line coincide at $\Delta r = 0.04$ as shown in Fig. 16b and 16c, demonstrating that all the states have approximately the same average value of z (as discussed above), as well as the same distribution. The distribution gets narrower as the coarse-graining parameter l increase from $l = 2$ to $l = 4$ as shown in Fig. 16c. On the other hand Z changes as the friction changes following the isostatic condition, as seen in Fig. 16a. This is in good agreement with the theory.

Along the RLP line, the situation is analogous. As discussed above, $z \approx Z$. This is clearly demonstrated in Fig. 17b which should be compared with the analogous Fig. 16b for the RCP line. Figure 17a also shows how Z changes with friction in the same way as in Fig. 16a. More importantly, we find that the bounds of $\langle z \rangle_l$ are well approximated between the bounds proposed by the theory ($Z, 6$). The slight shift towards higher coordinations observed in Fig. 17b is due to the approximate nature of our measurements from real packings and the small increment in volume fraction from the critical point of jamming, as discussed above. Overall, we conclude that along the RCP line, all states have $z \approx 6$, with Z changing from 6 to 4 as friction is increased. On the other hand, along the RLP line, we find that $z \approx Z$. These two results confirm the theory very well. Figure 18 summarizes all these findings indicating the ranges of z and Z along the iso- X lines of RCP and RLP, the iso- z vertical lines, and the iso- Z horizontal lines in the phase diagram.

8. Outlook

We have presented several results in the disordered sphere packing problem and here will discuss their significance. We start with the results that we believe are more robust and may survive higher scrutiny, and follow with the results that require further study plus a discussion on how to improve the theory.

The final result of the phase diagram, the characterization of RCP and RLP using the compactivity, the role of friction in the determination of the limiting packings are interesting results, almost independent of the theory. The distinction between the geometrical and mechanical coordination number is also important, allowing for the implementation of averages in the partition function. On the mathematical side, the microscopic volume function and the formula obtained for the Voronoi cell in Jamming I [49] are important and exact results which are the foundation of all preceding work presented herein.

While the predictions Eqs. (24) and (25) of RCP and RLP approximate very well the known values, they are obviously not exact expressions, since they are based on several approximations of the statistical theory of volumes. Thus, the

implementation of the mesoscopic volume function and the probability distribution of volumes on which these results are based are, perhaps, the points where improvements may be necessary. While the $\frac{2\sqrt{3}}{z}$ formula reproduces the average volume fraction surprisingly well, it is based on approximations to calculate the probability distribution of volumes, $P_{>}(c)$, as explained in Jamming I [49]. More work is needed to obtain better approximations to such a distribution to capture not only the mean value of the Voronoi volume but higher moments as well. A full discussion is performed in Jamming IV [52]. The present theory shows the way to improve upon Jamming I and obtain an exact formulation of $P_{>}(c)$, at least to a prescribed value of the coordination shell. Such a formulation is presently being developed and is based on a systematic study of quasiparticles with fixed geometrical coordination number; it produces good fits of $P(\mathcal{W}_i^s)$ for the case of 2d, while 3d calculations are under way.

Other approximations that require additional attention are the considerations leading to the density of states $g(z)$. While the main results of RCP and RLP are nearly independent of the particular form of $g(z)$, other quantities such as the entropy and the equations of state for finite nonzero compactivity are more sensitive to it. By a direct measurement of the entropy, $g(z)$ can be calculated and compared to the simple exponential form used in the present study.

Furthermore, we have explicitly removed crystal states from our calculations by considering the upper bound of $z = 6$. A more general theory is needed then to investigate the transition from the RCP to the FCC as crystals starts to form in the system. Such a theory will include not only disordered states but also partially crystallized states and would give $X = 0$ at FCC following the full Edwards partition function, Eq. (5). We investigate this idea in [69], where we find that RCP can be interpreted as the “freezing point” in a first-order phase transition between ordered and disordered packing phases.

The distribution of coordination number, assumed to be a delta function, is another approximation to be improved upon. Once again, this may not affect the predicted RCP and RLP but deeper studies require also a distribution of z . A more general ensemble is being considered that predicts the distribution of z in good agreement with the existing data (see Jamming IV [52]).

Finally, the extension to study the microstates requires more investigation. The identification of the elementary units as quasiparticles of fixed coordination number is interesting and could eventually lead to more precise solutions of RCP and RLP.

9. Conclusions

In conclusion, using Edwards statistical mechanics we have elucidated some aspects of RLP and RCP in the disordered spherical packing problem. The numerical results suggest a way to experimentally test the existence of the predicted packings. By allowing the grains to settle in liquids of varying density, the speed of the particles can be varied and a systematic exploration of the jamming phase diagram can be achieved.

Beyond the elucidation of some questions in the sphere packing problem, other problems can now be addressed systematically from the point of view of what we have learned from the phase diagram. This includes the investigation of the criticality of the jamming transition from frictionless to frictional systems by extending the phase space to (ϕ, Z, σ) , and generating packings away from the isostatic plane by isotropically compressing the packings generated in the plane of Fig. 4. Previous studies have focused on the frictionless point and on fixed friction. According to our results it is important to sample all the phase space for different friction and compactivities according to the preparation protocols explained above.

Previous results find power law scaling [29, 30, 27, 32] where the stress vanishes as $\sigma \sim (\phi - \phi_c)^\alpha$. A possible scenario is depicted in the extended phase diagram of Fig. 19 in the 3-dimensional space (ϕ, Z, σ) , which could be tested numerically and experimentally. We note in passing that, all the results in the present study refer to the isostatic plane at the jamming transition $\sigma = 0$ or hard sphere limit. We expect that, as we compress packings of soft spheres, different planes of $\sigma = \text{constant} \neq 0$ will be obtained as shown in Fig. 19. These compressed states are described not only by the compactivity X but also the angoricity A through the full partition function in the VF ensemble, Eq. (2). Our preliminary results indicate that there seems to be evidence of criticality as the isostatic plane is approached when $\sigma \rightarrow 0$, although with exponents dependent on friction as well as the value of the compactivity.

Additional topics to be addressed by means of the presented approach include characterization of jamming in the phase space of configurations, the problem of elasticity and Green's function and the study of the pair correlation function $g(r)$, the volume distribution $P(\mathcal{W}_i^s)$, Voronoi volume, $P(\mathcal{W}_i^{\text{vor}})$, and coordination number $P(z)$, which are within the reach of the present approach. Other systems under consideration are two-dimensional systems [53], polydisperse systems [54], as well as the mean field case of infinite dimension. These are interesting cases, since there are many questions debated as to what is the more dense state in higher dimension. Extensions to other systems such as anisotropic particles are also within the reach of the present approach.

Finally, a complete characterization of the VF-ensemble can now be performed through the measurement of other quantities as a function of the volume fraction, such as the force distribution $P(F_n, F_t)$, and equations of state through the angoricity in the (ϕ, Z, σ) space. Some of these quantities can be obtained analytically from the ensembles allowing for interesting predictions.

The phase diagram introduced here serves as a beginning to understand how random packings fill space in 3d. The comparative advantage of the present approach over extensive work done in the past, is in the classification of all packings through X , Z and ϕ in the theoretical phase diagram from where these studies could be systematically performed. This classification guides the search for indications of jamming from a systematic point of view, through the exploration of all jammed states from $\mu = 0$ to $\mu \rightarrow \infty$.

Acknowledgements. This work is supported by the National Science Foundation, CMMT Division and the Department of Energy, Office of Basic Energy

Sciences, Geosciences Division. We are grateful to B. Brujić and A. Yupanqui for inspirations, C. Briscoe for a critical reading of the manuscript and the hospitality of UFC, Fortaleza where part of this work was done.

References

- [1] T. C. Hales, <http://arxiv.org/abs/math.MG/9811078>.
- [2] A. Thue, *Forandlingerneved de Skandinaviske Naturforskeres*, **14**, 352-353 (1892).
- [3] A. Thue, *Christinia Vid. Selsk. Skr.* **1**, 1-9 (1910).
- [4] J. D. Bernal, and J. Mason, *Nature* **188**, 910 (1960); J. D. Bernal, *Nature*, 185 (1960); J. D. Bernal, *Proc. Roy. Soc. London, Ser. A* **280**, 299 (1964).
- [5] Anonymous, *Nature* **239**, 488 (1972).
- [6] G. D. Scott, and D. M. Kilgour, *Brit. J. Appl Phys (J. Phys. D)* **2**, 863-866 (1969); G. D. Scott, *Nature*, **188**, 908 (1960).
- [7] J. L. Finney, *Proc. Roy. Soc. London, Ser. A* **319**, 479 (1970).
- [8] J. D. Berryman, *Phys. Rev. A* **27**, 1053-1061 (1983).
- [9] G. Y. Onoda, and E. G. Liniger, *Phys. Rev. Lett.* **64**, 2727 (1990).
- [10] S. Torquato, T. M. Truskett, P. G. Debenedetti, *Phys. Rev. Lett.* **84**, 2064 (2000).
- [11] R. P. Behringer and J. T. Jenkins, eds., *Powders & Grains 97* (Balkema, Rotterdam, 1997).
- [12] A. Coniglio A, A. Fierro, H. Hermann and M. Nicodemi, eds, *Unifying concepts in granular media and glasses*, (Elsevier, 2004).
- [13] S. F. Edwards and R.B.S. Oakeshott, *Physica A* **157**, 1080-1090 (1989).
- [14] S. F. Edwards, The role of entropy in the specification of a powder, in *Granular matter: an interdisciplinary approach* (ed A. Mehta) 121-140, Springer-Verlag, New York, 1994.
- [15] R. Blumenfeld, and S. F. Edwards, *Phys. Rev. Lett.* **90**, 114303 (2002).
- [16] S. F. Edwards, *Physica A* **353**, 114 (2005).
- [17] M. P. Ciamarra, A. Coniglio, M. Nicodemi, *Phys. Rev. Lett.* **97**, 158001 (2006).
- [18] E. R. Nowak, J. B. Knight, E. BenNaim, H. M. Jaeger and S. R. Nagel, *Phys. Rev. E* **57**, 1971 (1998).

- [19] M. Schröter, D. I. Goldman, H. L. Swinney, *Phys. Rev. E* **71**, 030301(R) (2005).
- [20] J. Brujić, P. Wang, D. L. Johnson, O. Sindt, and H. A. Makse, *Phys. Rev. Lett.* **95**, 128001 (2005).
- [21] E. Bertin, O. Dauchot and M. Droz, *Phys. Rev. Lett.* **96**, 120601 (2006).
- [22] L. F. Cugliandolo, J. Kurchan, L. Peliti, *Phys. Rev. E* **55**, 3898 (1997).
- [23] A. Barrat, J. Kurchan, V. Loreto, M. Sellitto, *Phys. Rev. Lett.* **85**, 5034 (2000).
- [24] H. A. Makse and J. Kurchan, *Nature* **415**, 614 (2002).
- [25] A. Fierro, M. Nicodemi, M. Tarzia, A. de Candia, A. Coniglio, *Phys. Rev. E* **71**, 061305 (2005).
- [26] A. Liu and S. R. Nagel, *Nature* 396, 21-22 (1998).
- [27] H. A. Makse, D. L. Johnson, L. M. Schwartz, *Phys. Rev. Lett.* **84**, 4160 (2000).
- [28] V. Trappe, V. Prasad, L. Cipelletti, P. N. Segre, D. A. Weitz, *Nature* **411**, (2001).
- [29] C. S. O'Hern, S. A. Langer, A. J. Liu, and S. R. Nagel, *Phys Rev. Lett.* **88**, 075507 (2002).
- [30] L. E. Silbert, D. Ertas, G. S. Grest, T. C. Halsey, D. Levine, *Phys. Rev. E* **65**, 031304 (2002).
- [31] C. S. O'Hern, L. E. Silbert, A. J. Liu, and S. R. Nagel, *Phys. Rev. E* **68**, 011306 (2003).
- [32] H. Zhang and H. A. Makse, *Phys. Rev. E* **72** 011301, (2005).
- [33] T. Under, J. Kertesz, and D. E. Wolf, *Phys. Rev. Lett.* **94**, 178001 (2005).
- [34] K. Shundyak, M. van Hecke and W. van Saarloos, *Phys. Rev. E* **75**, 010301 (2007).
- [35] L. D. Landau and E. M. Lifshitz, *Theory of Elasticity*, (Pergamon, NY, 1970).
- [36] R. D. Mindlin, *J. Appl. Mech. (ASME)* **71**, (1949).
- [37] J. Brujić, S. F. Edwards, D. V. Grinev, I. Hopkinson, D. Brujić, and H. A. Makse, *Faraday Discuss.* **123**, 207 (2003).
- [38] G. Parisi, and F. Zamponi, *Rev. Mod. Phys.* **82**, 789-845 (2010).
- [39] B. D. Lubachevsky and F. H. Stillinger, *J. Stat. Phys.* **60**, 561 (1990).

- [40] M. Skoge, A. Donev, F. H. Stillinger, and S. Torquato, *Phys. Rev. E* **74**, 041127 (2006).
- [41] F. Krzakala and J. Kurchan, *Phys. Rev. E* **76**, 021122 (2007).
- [42] P. Philippe, and D. Bideau, *Europhys. Lett.* **60**, 677 (2002).
- [43] S. Henkes and B. Chakraborty, *Phys. Rev. Lett.* **95**, 198002 (2005).
- [44] R. Blumenfeld, On entropic characterization of granular materials, in *Lecture Notes in Complex Systems Vol. 8: Granular and Complex Materials*, 43-53, eds (2007).
- [45] H. A. Makse, J. Brujić, and S. F. Edwards, *Statistical Mechanics of Jammed Matter*, in *The Physics of Granular Media*, edited by H. Hinrichsen and D. E. Wolf (Wiley-VCH, 2004).
- [46] T. Aste, M. Saadatfar, T. J. Senden, *J. Stat. Mech.*, P07010 (2006).
- [47] F. Lechenault, F. da Cruz, O. Dauchot, and E. Bertin, *J. Stat. Mech.*, P07009 (2006).
- [48] L. D. Landau and E. M. Lifshitz, *Statistical Physics* (Pergamon, NY, 1970).
- [49] C. Song, P. Wang, Y. Jin, and H. A. Makse, *Physica A* (2010), doi:10.1016/j.physa.2010.06.043.
- [50] C. Song, P. Wang, and H. A. Makse, *Nature* **453**, 629 (2008).
- [51] C. Briscoe, C. Song, P. Wang, and H. A. Makse, *Physica A* **389**, 3978 (2010).
- [52] P. Wang, C. Song, Y. Jin, and H. A. Makse, e-print arXiv:0808.2198.
- [53] S. Meyer, C. Song, Y. Jin, K. Wang, H.A. Makse, *Physica A* (2010), doi:10.1016/j.physa.2010.07.030.
- [54] M. Danisch, Y. Jin, and H. A. Makse, *Phys. Rev. E* **81**, 051303 (2010).
- [55] J. A. van Meel, B. Charbonneau, A. Fortini, and P. Charbonneau, *Phys. Rev. E* **80**, 061110 (2009).
- [56] R. C. Ball and R. Blumenfeld, *Phys. Rev. Lett.* **88**, 115505-1 (2002).
- [57] R. Blumenfeld, *Eur. Phys. J. B* **29**, 261 (2005).
- [58] J. Zhou, S. Long, Q. Wang, *Science* **312**, 1631 (2006).
- [59] S. Alexander, *Phys. Rep.* **296**, 65 (1998).
- [60] C. F. Moukarzel, *Phys. Rev. Lett.* **81**, 1634 (1998).
- [61] S. F. Edwards and D. V. Grinev, *Phys. Rev. Lett.* **82**, 5397 (1999).

- [62] S. Torquato, F. H. Stillinger, *J. Phys. Chem B* **105**, 11849 (2001).
- [63] J. Brujić, C. Song, P. Wang, C. Briscoe, G. Marty, and H. A. Makse, *Phys. Rev. Lett.* **98**, 248001 (2007).
- [64] F. H. Stillinger, *Science* **267**, 1935-1939 (1995).
- [65] H. A. Makse, N. Gland, D. L. Johnson, and L. M. Schwartz, *Phys. Rev. Lett.* **83**, 5070 (1999);
- [66] H. A. Makse, N. Gland, D. L. Johnson, and L. M. Schwartz, *Phys. Rev. E* **70**, 061302 (2004).
- [67] F. Zamponi, *Nature* **453**, 606 (2008).
- [68] S. Mukhopadhyay, M. L. Gilchrist, and H. A. Makse (in preparation).
- [69] Y. Jin and H. A. Makse, *Physica A* (2010), doi:10.1016/j.physa.2010.08.010.
- [70] F. Lechenault and K. E. Daniels, e-print arXiv:1001.5411.
- [71] C. Song, P. Wang, and H. A. Makse, *AIP Conf. Proc.* 1227, 271 (2010).
- [72] A. Donev *et al.*, *Phys. Rev. E* **71**, 011105 (2005).

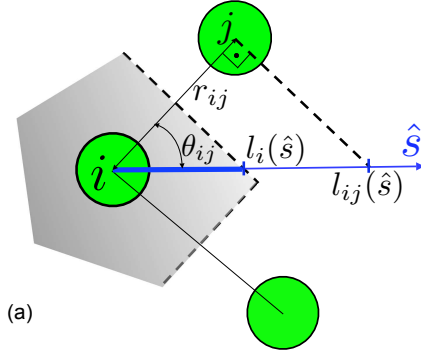


Figure 1: The Voronoi volume is the light grey area (shown in 2d for simplicity). The limit of the Voronoi cell of particle i in the direction \hat{s} is $l_i(\hat{s}) = r_{ij}/2 \cos \theta_{ij}$. Then the Voronoi volume is proportional to the integration of $l_i(\hat{s})^3$ over \hat{s} as in Eq. (6).

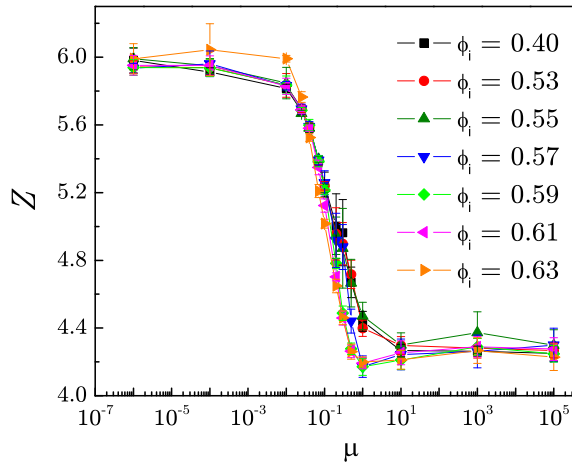


Figure 2: Mechanical coordination number versus friction μ obtained in our numerical simulations explained in Section 7 for different preparation protocols characterized by the initial volume fractions ϕ_i indicated in the figure. The symbols and parameters used in these simulations are the same as in the plot of Fig. 11.

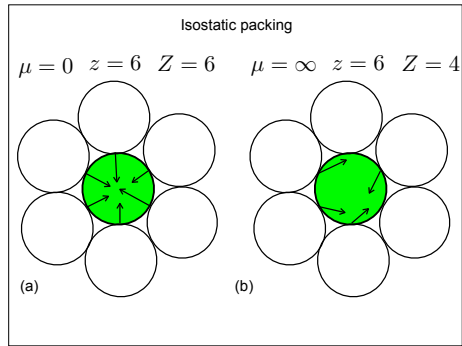


Figure 3: (a) Consider a frictionless packing at the isostatic limit with $z = 6$. In this case the isostatic condition implies also $Z = 6$ mechanical forces from the surrounding particles. (b) If we now switch on the tangential forces using the same packing as in (a) by setting $\mu \rightarrow \infty$, the particle requires only $Z = 4$ contacts to be rigid. Such a solution is guaranteed by the isostatic condition for $\mu \rightarrow \infty$. Thus, the particle still have $z = 6$ geometrical neighbors but only $Z = 4$ mechanical ones.

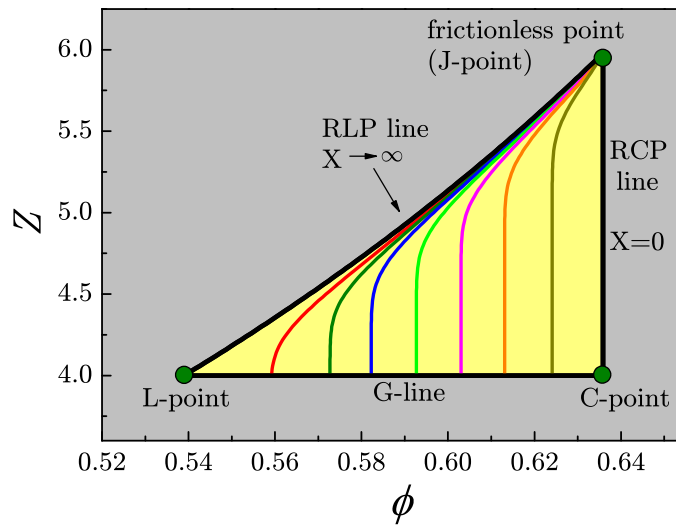


Figure 4: **Phase diagram of jammed matter: Theory.** Theoretical prediction of the statistical theory. All disordered packings lie within the yellow triangle demarcated by the RCP line, RLP line and G line. Lines of finite isocompactivity are in color. The grey area is the forbidden zone where no jammed packings can exist.

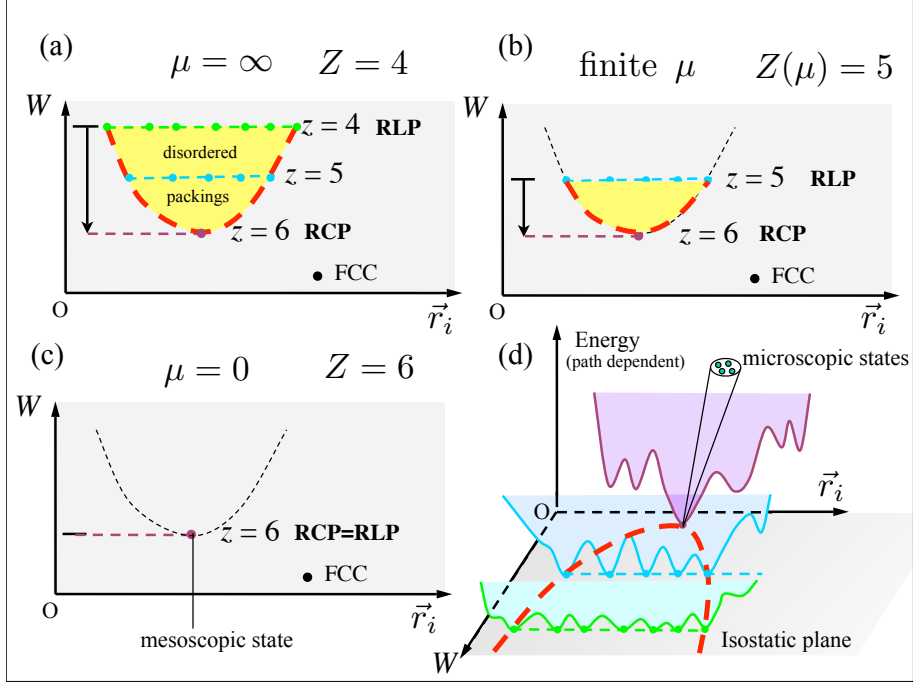


Figure 5: **Schematic representation of the volume landscape of jammed matter** (\vec{r}_i, W) . The multidimensional coordinate \vec{r}_i represents the degrees of freedom: the particle positions. Each dot represents a discrete mesoscopic jammed states at different z . It is important to note that for each meso state there are microscopic states with the same z . All disordered packings are in the yellow region (of an schematic shape) of the phase space which corresponds to the isostatic plane of hard spheres at the jamming transition where our calculations are performed. Other ordered packings have lower volume, such as the FCC. (a) We represent the case of $\mu = \infty$. The states represent those along the G-line in Fig. 4 as the compactivity varies from $X = 0$ (ground state) to $X \rightarrow \infty$ at the RLP. The horizontal lines indicate packings at constant volume. The ground state of jammed matter for this friction coefficient has $z = 6$ and the highest volume states are found for $z = 4$. The arrow indicates the limits of integration in the partition function for this particular friction. (b) For another finite μ , the space is delimited by above by a line of constant $z = Z(\mu)$. (c) For $\mu = 0$ only the ground state is available, giving rise to a single state. (d) The volume states states in (a,b,c) are separated by energy barriers represented by the third coordinate in the phase space. The energy barriers are path dependent due to friction between the particles. Nevertheless, the jammed configurations are well-defined in the isostatic plane, and the energy barriers represent the work done to go from one configuration to another. Only at the frictionless point, the energy barriers are path independent.

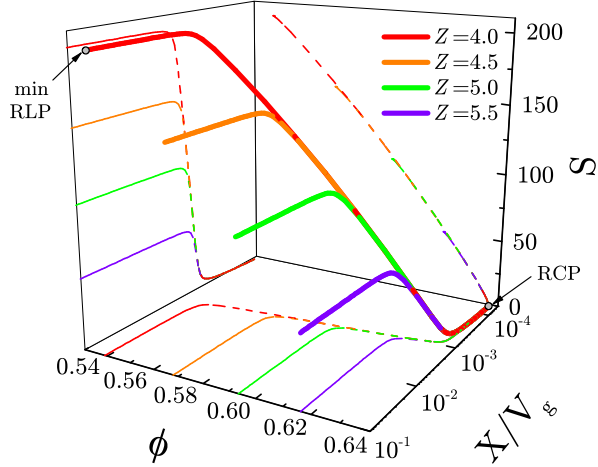


Figure 6: **Predictions of the equation of state of jammed matter in the (X, ϕ, s) space.** Each line corresponds to a different system with $Z(\mu)$ as indicated. The projections in the (ϕ, s) and (X, s) planes show that the RCP ($X = 0$) is less disordered than the RLP ($X \rightarrow \infty$). The projection in the (X, ϕ) plane resembles qualitatively the compaction curves of the experiments [18, 19, 20].

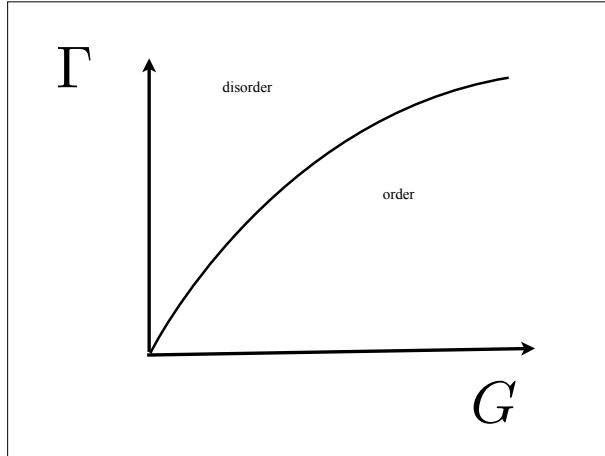


Figure 7: Dimensional analysis indicates that for finite shear modulus G of the particles, the system can crystallize or randomize according to the quenched rate Γ . This argument allows for a comparison with hard-sphere simulations that are done in the limit $G \rightarrow \infty$. In this case only $\Gamma \rightarrow \infty$ avoids partial crystallization.

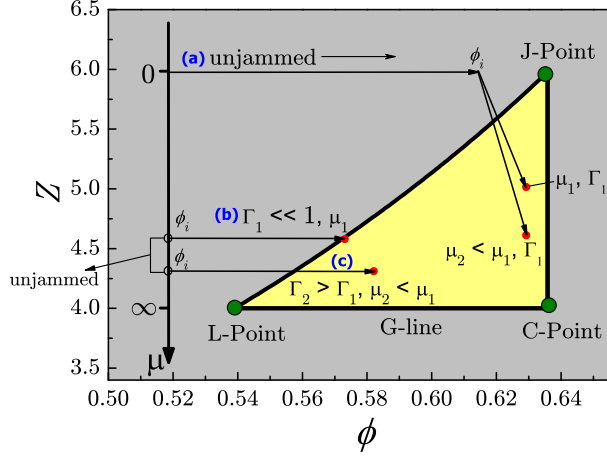


Figure 8: Schematic representation of the protocol used to dynamically achieved the packings in the phase diagram. (a) The region near the C-point (high friction, high volume fraction) is the most difficult to access. Here, we prepare an unjammed sample with no friction at ϕ_i ($=0.62$ in the diagram) very close to RCP, and then we switch friction to compress to the required frictional jammed state. The packing follow the paths indicated in the figure for two friction coefficients. On the other hand, the RLP-line is easily obtained by compressing unjammed packings with low ϕ_i ($=0.52$ in the diagram) at (b) a given compression rate Γ_1 for a given friction coefficient. (c) There is a small dependence on Γ , the faster the compression the deeper we enter in the phase diagram.

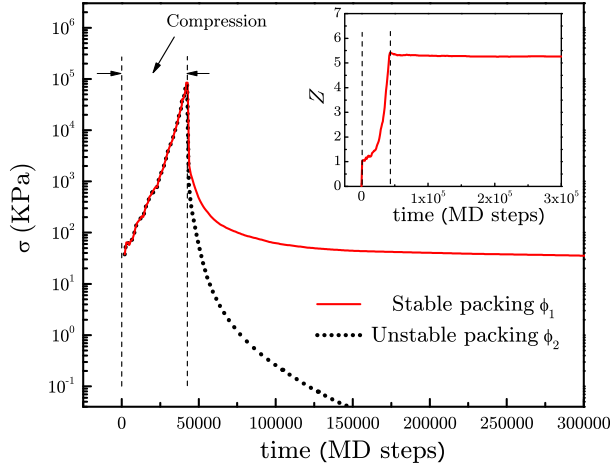


Figure 9: Time evolution of stress (the pressure in the system) for two packings simulated as explained in the text. The solid red line represents a packing with $\phi_1 > \phi_c$ and dotted black line represents a packing with $\phi_2 < \phi_c$, where $\phi_1 = \phi_2 + 2 \times 10^{-4}$. The inset shows the time evolution of the coordination number.

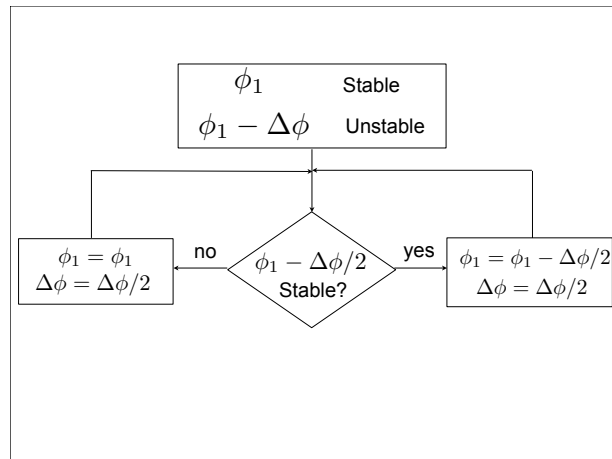


Figure 10: Flow chart for searching procedure of critical volume fraction ϕ_c .

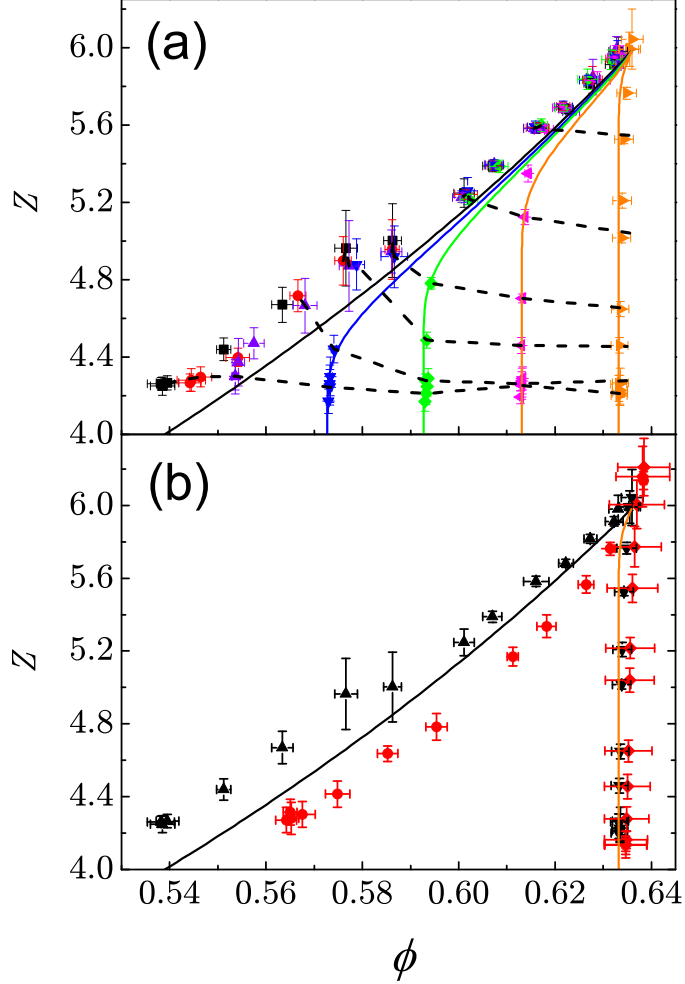


Figure 11: **Phase diagram of jammed matter: Simulations.** Numerical simulations demonstrate how to dynamically access the theoretically found states. The numerical protocol is parameterized by $(\phi_i, \Gamma, \eta, \mu)$. (a) The plot shows the dependence of the final jammed states (ϕ, Z) on ϕ_i for a fix $\Gamma = 10^{-7}$ and $\eta = 10^{-3}$ (except for the orange \blacktriangleright curve which is for $\eta = 10^{-4}$) from left to right $\phi_i = 0.40$ (black \blacksquare), 0.53 (red \bullet), 0.55 (violet \blacktriangle), 0.57 (blue \blacktriangledown), 0.59 (green \blacklozenge), 0.61 (pink \blacktriangleleft) and 0.63 (orange \blacktriangleright). Each equal-color line set represents a different ϕ_i and the dashed lines join systems with the same friction μ . Solid lines represent the theoretical results with $h_z = e^{-100}$ or $z_c = 0.01$ for different compactivities measured in units of $10^{-3}V_g$. From left to right $X = \infty$ (black solid line), 1.62 (blue solid line), 1.38 (green solid line), 1.16 (pink solid line) and 0.88 (orange solid line). The error bars correspond to the s.d. over 10 realizations of the packings. (b) The plot focuses on the dependence of (ϕ, Z) on (Γ, η) for two different ϕ_i . Solid black symbols are for $\phi_i = 0.40$ and $(\Gamma, \eta) = (10^{-7}, 10^{-3})$ (black \blacksquare) and $(10^{-4}, 10^{-4})$ (black \bullet). Open red symbols are for $\phi_i = 0.63$ and $(\Gamma, \eta) = (10^{-7}, 10^{-3})$ (red \square) and $(10^{-3}, 10^{-4})$ (red \circ).



Figure 12: Measuring the temperature of sand. Pictorial representation.

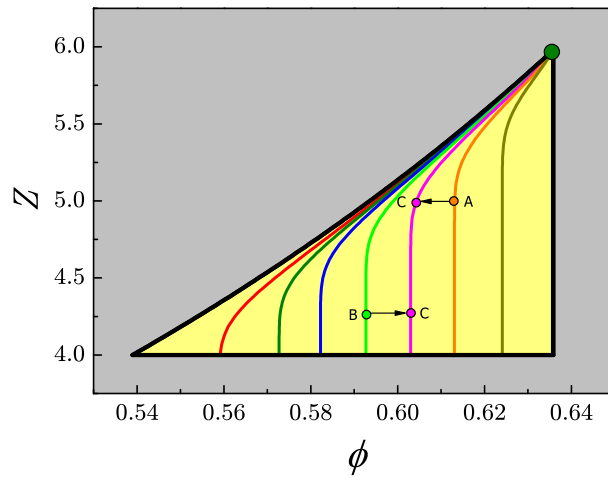


Figure 13: Sketch depicting a possible ABC experiment to test the zero-th law of granular thermodynamics and the validity of the phase diagram for finite compactivities. For intermediate frictions, the A and B systems should follow the arrows to C when put into contact and allow to interchange volume by gently shaking.

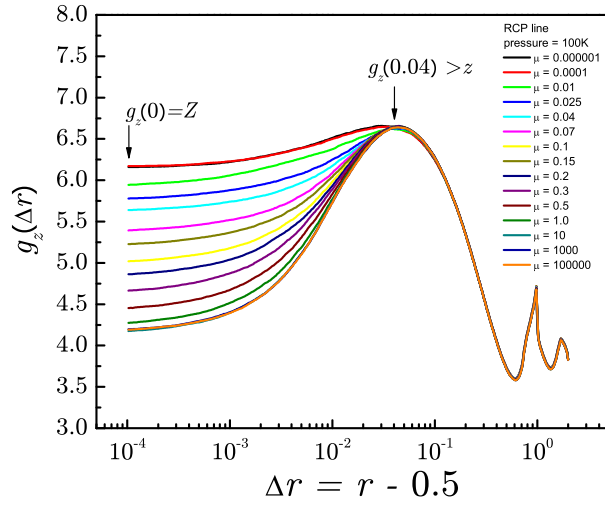


Figure 14: $g_z(\Delta r)$ of packings with various friction coefficient μ along RCP line. We set $2R = 1$.

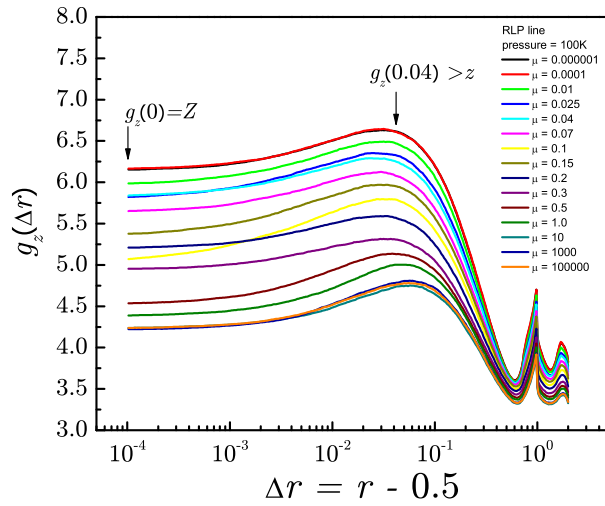


Figure 15: $g_z(\Delta r)$ of packings with various friction coefficient μ along RLP line.

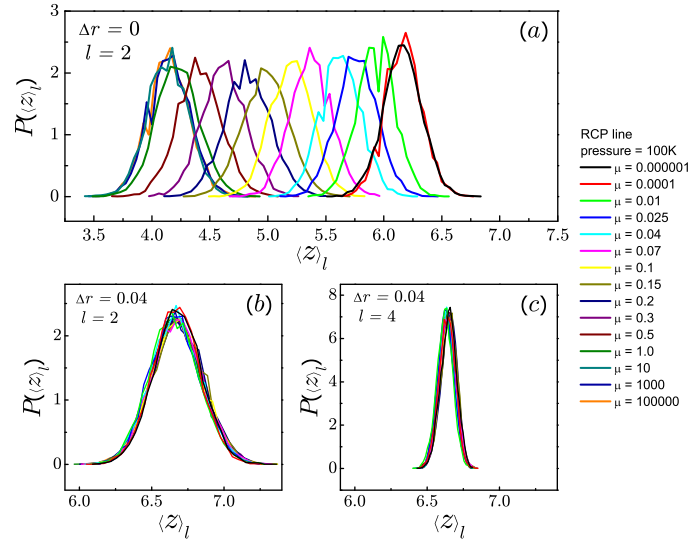


Figure 16: PDF of the coarse-grained coordination number $\langle z \rangle_l$ for packings with various friction coefficient μ along the RCP line. (a) $\Delta r = 0$ and $l = 2$; (b) $\Delta r = 0.04$ and $l = 2$; (c) $\Delta r = 0.04$ and $l = 4$.

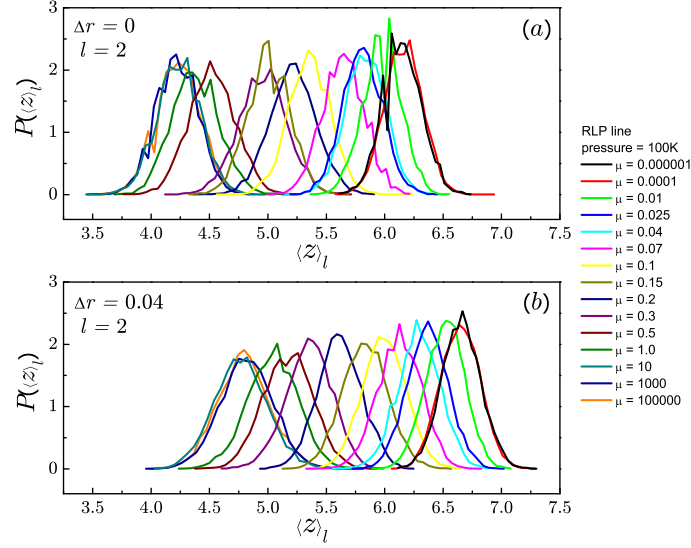


Figure 17: PDF of the coarse-grained coordination number $\langle z \rangle_l$ for packings with various friction coefficient μ along the RLP line. (a) $\Delta r = 0$ and $l = 2$; (b) $\Delta r = 0.04$ and $l = 2$.

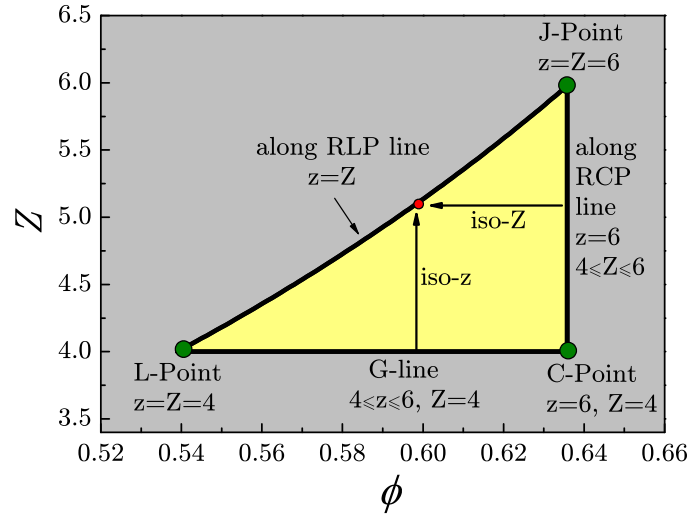


Figure 18: Summary of the theoretical findings regarding the range of z and Z along the different iso- z , iso- Z , and iso- X lines and the J, C, and L-points in the phase diagram.

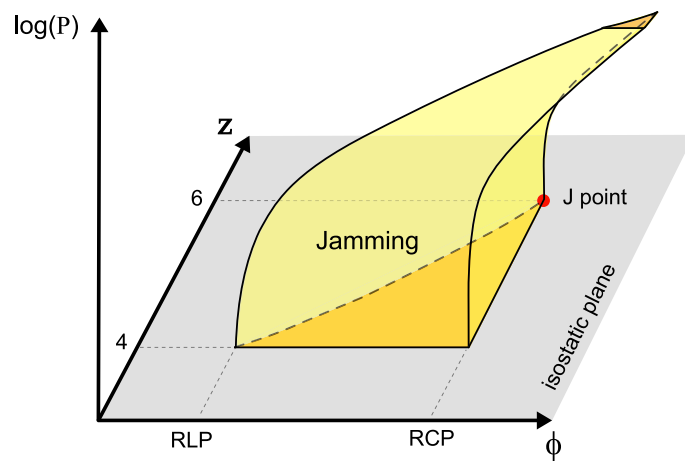


Figure 19: Sketch depicting a possible extension of the phase diagram of Fig. 4 in the (ϕ, Z) isostatic plane at the jamming transition to the full phase diagram in the (ϕ, Z, σ) space to investigate the criticality of the jamming transition for all packings with any friction coefficient.

